FACULDADE DE ENGENHARIA DA UNIVERSIDADE DO PORTO

Universidade do Porto

Faculdade de Engenharia

FEUP

Development of Multifunctional Nanoparticles for Targeted Therapy and Imaging of Rheumatoid Arthritis

Catarina da Costa Moura

bio08026@fe.up.pt

FEUP – Faculdade de Engenharia da Universidade do Porto, Rua Dr. Roberto Frias s/n, 4200-465 Porto, Portugal

Master Thesis
submitted in partial fulfilment of the requirements
for the Degree of Master of Science in BioEngineering
at the Faculty of Engineering, University of Porto

July 2013

- This Page was intentionally left blank. -

This work was submitted as a Master Thesis in partial fulfilment of the requirements for the degree of Master of Science in BioEngineering at the Faculty of Engineering, University of Porto.

It was conducted under the guidance of Professor Bruno Filipe Carmelino Cardoso Sarmento, PhD, Affiliated Researcher at INEB – Instituto de Engenharia Biomédica and Assistant Professor at Instituto Superior de Ciências da Saúde-Norte (ISCS-N), and under the co-supervision of Professor Maria de La Salette de Freitas Fernandes Hipólito Reis Dias Rodrigues, Associate Professor at Faculty of Pharmacy, University of Porto and Affiliated Researcher at GABAI – REQUIMTE.

The research experimental work was conducted at the Department of Chemical Sciences of the Faculty of Pharmacy, University of Porto, in collaboration with INEB and ISCS–N – Instituto Superior de Ciências da Saúde – Norte.

Thesis defense took place at the Faculty of Engineering, University of Porto, on the 15th July 2013. The Thesis Examination Committee was composed by Professor Sofia Teresa Coimbra Antunes Costa Lima, PhD, Principal Investigator at IBMC – Instituto de Biologia Molecular e Celular, Professor Ana Paula Pêgo, PhD, Principal Investigator at INEB, Professor Bruno Filipe Carmelino Cardoso Sarmento and Professor Maria de La Salette de Freitas Fernandes Hipólito Reis Dias Rodrigues. The Master Thesis was attributed a final score of 19 out of 20 possible points.

- This Page was intentionally left blank. -

Acknowledgments

I express my deepest and sincere gratitude to Professor Bruno Sarmento, for giving me the opportunity to work with his research group. For his guidance and inspiration shared everyday during my thesis research, and for giving me such encouragement to believe in myself.

I am deeply grateful to Professor Sallete Reis, for all support and promptness to help, and for welcoming me amongst her research group at the Faculty of Pharmacy.

To Metal&Bio and to Engineering for offering me the best times in my life. And to my family and closest friends who helped me with their friendship and support.

To my parents and sister who always supported all of my dreams and hopes, I thank you from the bottom of my heart. And I want to thank Miguel for his endless love, continuous support and encouragement during all this time.

- This Page was intentionally left blank. -

Abstract

Rheumatoid arthritis (RA) is one of the most common and severe autoimmune diseases related to joints. Regrettably, RA inflammatory process remains a puzzle, and finding effective therapies that specifically target RA revealed to be a daunting task. Inflammatory macrophages are persistent at the site of RA and frequently over-express the cell surface Fc receptor CD64, which is associated with the disease and motivates the search for a new targeted-therapy strategy for RA.

In this work, a ground-breaking approach for RA theranostics was proposed, taking advantage of the vast potential of nanomedicine. This study aimed the development of a nanoparticulate system for intravenous administration, based on PLGA (a biodegradable, FDA-approved polymer, renowned for its applications in medical research). The nanoparticles (NPs) comprised the co-encapsulation of both methotrexate (MTX) and iron oxide nanoparticles (SPIONs), for RA therapy and imaging, respectively. The nanoparticles were further functionalised with an anti-CD64 antibody to specifically target RA-associated macrophages, minimising damage to the surrounding tissues.

In total, eight different PLGA-based NPs were prepared in order to compare the effect of each component (MTX, SPIONs and antibody) on NP properties. Particle size was measured by dynamic, light scattering, as well as analysed by both scanning and transmission electron microscopy. Zeta potential was determined by phase analysis light scattering. Neither MTX nor SPIONs encapsulation significantly affected the NPs properties, though antibody conjugation caused an expected slight increase on both size and surface charge. Nevertheless, all nanoparticles presented sizes bellow 200 nm and charges lower than -16 mV, suggesting the potential applicability of the nanosystem for intravenous administration and RA theranostics.

TEM micrographs confirmed the encapsulation of SPIONs within the PLGA matrix. Successful antibody conjugation was also first suggested by TEM, in the appearance of a characteristic ‘corona’ surrounding the NPs. Both antibody conjugation and MTX encapsulation were confirmed by FT-IR and quantified by bicinchoninic acid assay (Micro BCA Kit) and HPLC, respectively, rendering encapsulation and conjugation values as high as 30 and 95%.

In vitro studies with a murine macrophage cell line (RAW 264.7) allowed drawing conclusions on the cytotoxic profile of the devised NPs. MTT and LDH assays indicated the high toxicity of MTX. Conversely, MTX-free NPs were only toxic when administrated at the highest concentration (1 mg/mL) supporting PLGA’s biocompatibility. Future work, using a human macrophage cell line, THP-1, will endorse studying the targeting capability of the anti-CD64 conjugated NPs aiming for the envisioned theranostics application.

This approach could bring a new insight for theranostic strategies, since targeted NPs are promising candidates for the future in nanomedicine. With this system the release and action of the drug could be enhanced and controlled, and potentially without injuring healthy tissues and organs, while simultaneously providing a non-invasive and specific imaging tool for RA.

Keywords: CD64; Drug Delivery; Imaging; Nanomedicine; Rheumatoid Arthritis; Targeted Therapy.

- This Page was intentionally left blank. -

Table of contents

- This Page was intentionally left blank. -

List of figures

- This Page was intentionally left blank. -

List of tables

- This Page was intentionally left blank. -

Glossary

BCA – Bicinchoninic Acid

BSA – Bovine Serum Albumin

DLS – Dynamic Light Scattering

DMARD – Disease-Modifying Antirheumatic Drug

DMEM – Dulbecco's Modified Eagle's Medium

DMSO – Dimethyl Sulfoxide

EDC – 1-Ethyl-3-(3-dimethylaminopropyl) Carbodiimide Hydrochloride

EMA – European Medicine Agency

FBS – Fetal Bovine Serum

FcγRI – Fc-Gama-Receptor I

FDA – Food and Drug Administration

FEUP – Faculdade de Engenharia da Universidade do Porto

FLS – Fibroblast-Like Synoviocyte

FT-IR – Fourier Transform Infrared

GABAI – Grupo de Análises Bioquímicas Ambientais e Industriais

HBSS – Hanks' Balanced Salt Solution

HPLC – High Performance Liquid Chromatography

IBMC – Instituto de Biologia Molecular e Celular

ISCS-N – Instituto Superior de Ciências da Saúde – Norte

Ig – Immunoglobulin

IL-8 – Interleukin-8

INEB – Instituto de Engenharia Biomédica

IONP – Iron Oxide Nanoparticle

LDH – Lactate dehydrogenase

mAb – Monoclonal Antibody

MES – 2-Morpholinoethanesulfonic Acid

MLS – Macrophage-Like Synoviocyte

MMP – Matrix Metalloproteinase

MRI – Magnetic Resonance Imaging

MTT – Thiazolyl Blue Tetrazolium Bromide

MTX – Methotrexate

NHS – N-Hydroxysulfosuccinimide

NP – Nanoparticle

PBS – Phosphate Buffer Saline

PdI – Polydispersity Index

PEG – Polyethylene Glycol

PhD – Philosophiæ Doctor

PLGA – Poly (Lactic-co-Glycolic Acid)

PVA – Poly (vynil alcohol)

RA – Rheumatoid Arthritis

REQUIMTE – Rede de Química e Tecnologia

SEM – Scanning Electron Microscopy

SLN – Solid Lipid Nanoparticle

SPION – Superparamagnetic Iron Oxide Nanoparticle

TEM – Transmission Electron Microscopy

TNF-α – Tumour Necrosis Factor-Alpha

1. Introduction

1.1. Histology and physiology of the joint

Joints play a vital role on humans' movements. While making the skeleton flexible and dynamic, they simultaneously contribute to the human body stability and protection. A joint occurs where two bones meet and, according to its structure, can be classified into three different categories: i) fibrous, ii) fibrocartilaginous or iii) synovial [1].

Fibrous joints are immovable. They consist of two bones connected by fibrous ligaments – a dense connective tissue rich in collagen. Skull sutures are amongst the best examples of fibrous joints – the dome of the skull must be immovable to protect the brain, therefore a joint of fibrous tissue exists between the bony plates [1, 2].

Fibrocartilaginous joints, in their turn, are slightly movable. Bones are held together with both fibrous connective tissue and cartilage as happens, for instance, in intervertebral discs. Each vertebra moves relatively to both vertebrae above and below it, conferring flexibility to the spine [1, 2].

Contrasting with the aforementioned examples, there are joints which are completely movable, known as synovial joints. These joints are undoubtedly the most common in the human body, and can be found in several structures such as the wrists, ankles, knees, shoulders, among others. They comprise an array of characteristic constituents, which are described below (Figure 1):

1. *Joint capsule*, with a smooth, non-adherent protein and crystalloid-permeable surface, which seals and surrounds the joint space;

2. *Synovial membrane or synovium*, constituted by fibrous tissue and the synovial intimal lining. The intimal lining is only one or two cell layers deep, containing two cell types, macrophage-like synoviocytes (MLS) and fibroblast-like synoviocytes (FLS), and works as an interface between the synovium and the synovial cavity;

3. *Synovial fluid*, retained on the synovial cavity, is an extremely viscous lubricating liquid secreted by the synovial cells. While FLS are responsible to release hyaluronan into the synovial cavity, in order to help retain fluid in the joint, the MLS have the important role of removing undesirable substances or metabolic wastes from the synovial fluid. This fluid, being highly hydrated and comprising hyaluronan molecules, lubricin and surface-active phospholipids, allows human movements to be painless by decreasing the friction between the two bones;

4. *Hyaline cartilage*, known as articular cartilage, which protects the ends of the articulating bones, providing a low friction coefficient between articular cartilages [1-4].

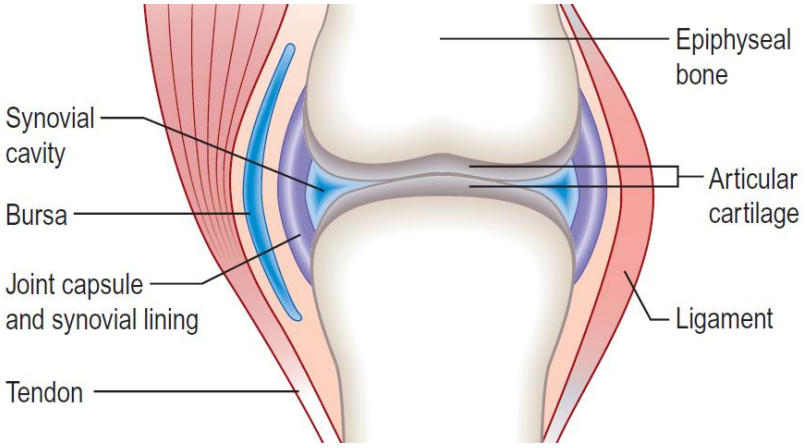

Figure 1 – Schematic diagram of a synovial joint. Adapted from [1].

1.2. Rheumatoid Arthritis

Rheumatoid arthritis (RA) is one of the most common and severe autoimmune diseases related to joints and affects 1% of the population around the globe [3, 5]. This chronic autoimmune inflammatory disease, in which the immune system attacks healthy tissue lining the joints, leads to functional disability and reduced quality of life, forasmuch as there is bone and cartilage destruction, joint swelling and pain [6]. Although this condition can occur in people at any time of their live, its prevalence significantly increases with age (bearing an average incidence age of 55 years-old) and the symptoms frequently develop in a gradual manner [5, 7].

The inflammation of RA begins in the synovium. Although there are several associated mechanisms that trigger the RA inflammatory response – such as lymphocytes activation, cytokine networks and production of pro-inflammatory molecules –, the pathway that leads to it is still unidentified. The foremost enigma of RA is to explain the reason underlying the fact that the synovium is the major target of the disease. Several investigation groups are investigating this unknown event in order to find a successful solution for an efficient early diagnosis and effective treatments [3, 8].

As a response to RA inflammation, the synovial tissue shows synovial lining hyperplasia as a result of FLS and MLS accumulation. In fact, the synovial intimal lining in RA, instead of one or two cells deep, is frequently up to five-fold deeper. These macrophage- and fibroblast-like cells promote inflammation producing chemical mediators such as pro-inflammatory cytokines, like the tumour necrosis factor-alpha (TNF-α), chemokines, as interleukin-8 (IL-8), and proteinases, counting with matrix metalloproteinases (MMPs) as an example. Consequently, more macrophages, lymphocytes, and fibroblasts are activated and the RA inflammatory process remains [3, 9, 10].

Unfortunately, RA often carries severe consequences in the patient's life quality since there are both cartilage and bone destruction (Figure 2). The pannus, where the synovial lining erodes into the bone, contains macrophages, fibroblasts and osteoclasts which contribute to joint damage. Added to the synovial hyperplasia, infiltration of inflammatory cells and joint destruction mentioned above, there is also formation of an extensive neo-vascular network that is permissible for the delivery of new chronic inflammatory cells to the joint. The development of new blood vessels, crucial for the proliferation of the synovial pannus, is induced by the unbalance between angiogenesis inducers and inhibitors. Chemokines and cytokines, produced by FLS and MLS, were identified as the most important inducers of angiogenesis in RA [9, 11, 12].

Since the RA inflammatory process remains unclear, finding effective therapies that specifically targets the autoimmune processes in the RA pathogenesis has turned out as being extremely challenging and, therefore, they are still non-existent. Recent studies have proposed that insufficient apoptosis of synovial inflammatory cells, especially macrophages, might contribute to the persistence of RA [9, 11]. Consequently, more research needs to be conducted to develop bolder strategies for creating effective means for early RA diagnosis and major long-term goals of successful treatment, aiming for the prevention of both joint destruction and associated comorbidities.

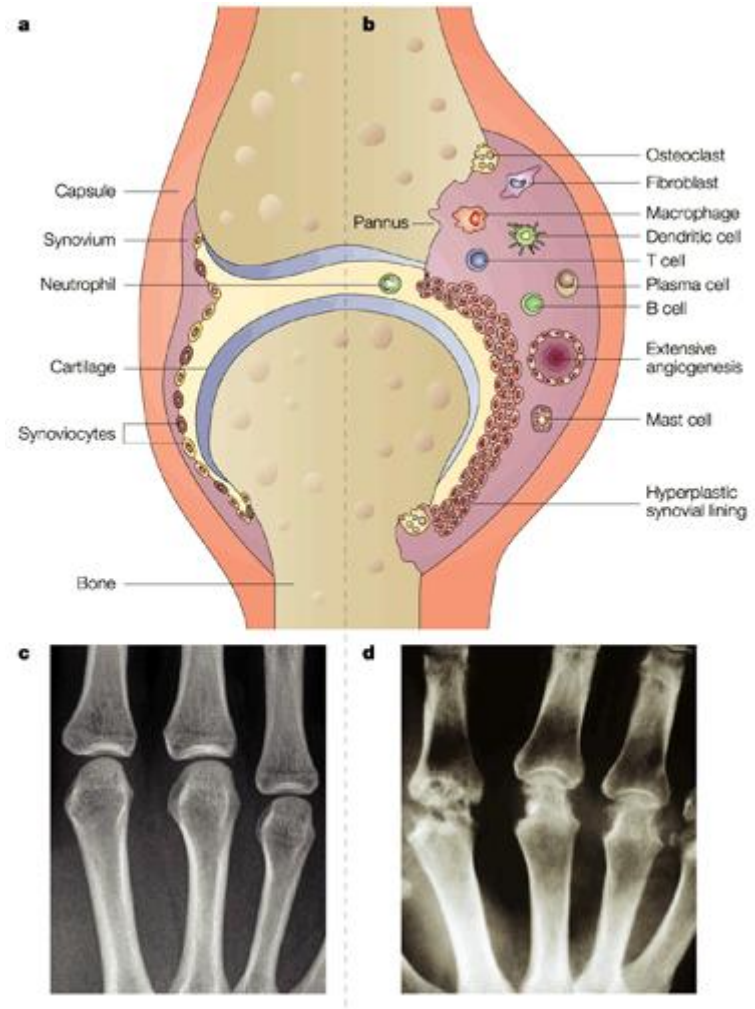

Figure 2 – (a) Schematic diagram of a healthy synovial joint. **(b)** Schematic diagram of a synovial joint with RA. **(c)** Radiograph of healthy metacarpophalangeal joints. **(d)** Radiograph of metacarpophalangeal joints with RA. Adapted from [13].

To accomplish a prompt treatment, an early diagnosis is required. However, diagnosing early RA can be a demanding task considering that one cannot confirm the presence of this autoimmune disease by a single test, needing to use several different criteria to provide an accurate diagnosis, including blood tests and X-ray analysis [14].

Magnetic resonance imaging (MRI) is arising as an invaluable technique in the examination of RA patients, since MRI has the ability to detect the earliest pathological changes around the joint. This technique produces a direct visualisation of the joint, and allows the identification of the earliest inflammatory changes. This remarkable and promising diagnosis approach augments the diagnosis speed and accuracy. Additionally, it is useful to choose the most suited treatment, as well as to monitor its response accordingly and to measure the disease evolution [15, 16].

Currently, the main target of RA therapy is to control the inherent inflammatory response and alleviate pain. Several therapeutic options have been used to manage and slow down the progression of the disease, which include the use of sulfasalazine, hydroxychloroquine or methotrexate – a first line disease modifying antirheumatic drug (DMARD) [6, 17]. This drug, methotrexate (MTX), is being widely used due to its satisfactory safety profile, efficacy and low cost. It is an analogue of folic acid as it disrupts cellular folate metabolism by inhibiting its target enzyme, dihydrofolate reductase [17-19].

Unfortunately, these strategies are still not definitive; as not being targeted, they suffer from non-specific distribution and drug accumulation in healthy tissues producing, consequently, harmful side effects [20, 21].

1.3. Nanomedicine

Nanotechnology, a forefront multidisciplinary research field, concerns the study of devices usually ranging the 1–100 nm, though larger systems, up to 1000 nm, may also be considered. As a consequence of its vast success on the development of biocompatible colloidal systems, such as nanoparticles (NPs), nanocapsules, micellar systems and conjugates, nanomedicine has thrived and is now providing new possibilities for the use of nanomaterials in medical applications for drug delivery and tissue regeneration [20, 22, 23].

Nanomedicine may also offer new opportunities to combine diagnosis and therapy in a single approach. Improved theranostics processes are being studied in order to develop new means to diagnose, fight and follow disease. There are different examples of nanomedicine-based approaches for simultaneous diagnosis and targeted therapy, based on quantum dots [24], chitosan NPs [25], liposomes [26] and iron oxide nanoparticles [27], among several others.

A new wave of medical innovation is emerging due to the possibility of multi-functionalization in nanomedicine-based strategies (Figure 3). NPs may have the ability to i) carry therapeutic agents, ii) be conjugated to a specific ligand, such as antibodies, to target a specific tissue or organ, iii) amplify imaging signal, by way of a co-encapsulated contrast enhancer, and iv) avoid bio-barriers and macrophage uptake, using for example polyethylene glycol (PEG) [20, 21, 23].

Targeted delivery systems are only possible due to both the discovery of novel specific receptors, which are exclusive or overly expressed in specific tissues, and the development of new ligand-conjugation techniques. These systems result in higher bioavailability of the therapeutic agent at the desired tissue, minimising side effects [20-23].

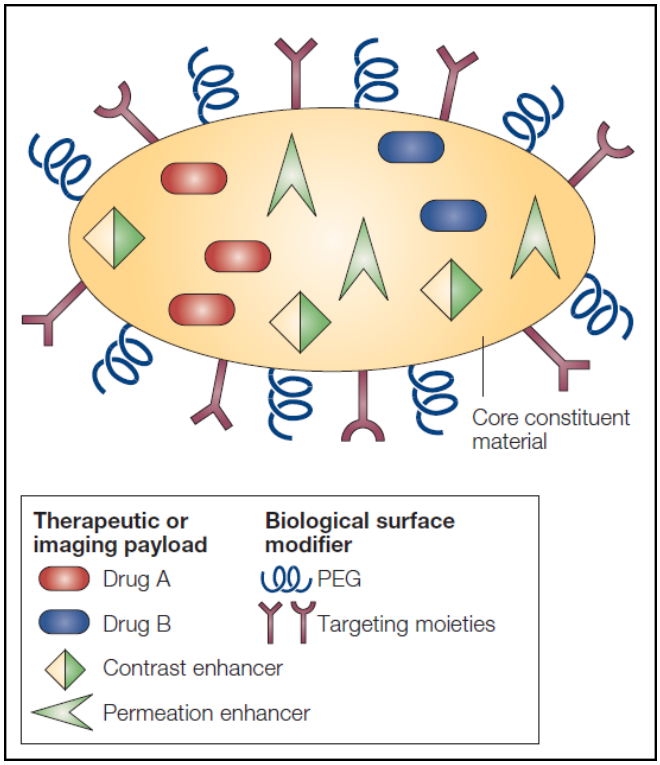

Figure 3 – Multifunctional nanoparticle illustration. Adapted from [20].

Iron oxide NPs are attractive nanosystems because of their peculiar physical properties, biocompatibility, inexpensiveness, and their ability to target specific locations, minimising damage to peripheral organs [28]. These magnetic NPs can be co-encapsulated along with drug molecules into NPs of other material such as poly (lactic-co-glycolic acid) (PLGA). Being a well-defined, biodegradable and biocompatible polymer, PLGA has attracted great attention: iron oxide NPs, when co-encapsulated into drug-loaded PLGA NPs, become protected from degradation and the drug release can be sustained and controlled. Also, there is the possibility to modify these NPs surface properties to provide stealth and selectivity to specific cells, organs or tissues. Moreover, iron oxide NPs can be used as imaging contrast agents, illustrating the application of nanotechnology to medical monitoring and diagnosis [23, 29].

- This Page was intentionally left blank. -

2. State of the art and rationale of the thesis

2.1. Drug delivery systems based on poly (lactic-co-glycolic acid) nanoparticles

Poly (lactic-co-glycolic acid), or PLGA, is a synthetic polymer which is renowned for its success among biodegradable micro and nanosystems. It results from the polymerisation reaction between glycolic and lactic acid monomers forming a random co-polymer (Figure 4) [29, 30].

As previously referred, drug delivery systems based on PLGA are of particular interest owing to their biodegradability and biocompatibility. In fact, PLGA copolymers degrade in the body by hydrolytic cleavage of ester links between lactic and glycolic acid, resulting in two biodegradable metabolite monomers. The human body deals effortlessly with these two hydrolysis products which are easily metabolised and eliminated as common metabolic waste products: carbon dioxide and water. Therefore, a minimal systemic toxicity is associated with the use of PLGA either for biomaterial applications or drug delivery [29, 31, 32].

Additionally, PLGA is an approved polymer for drug delivery systems for parenteral administration by both the American Food and Drug Administration (FDA) and the European Medicine Agency (EMA). Consequently, there are many approaches to various drug delivery systems and well-described formulations adapted to different types of drugs. PLGA copolymers have also the advantage of being well characterised as there are already commercially available medicines based on PLGA microparticles, like Lupron® and Zoladex® [29, 32].

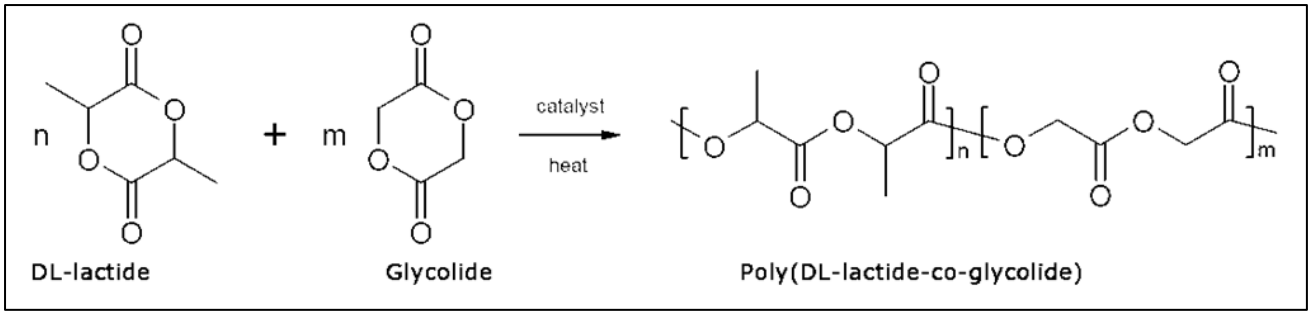

Figure 4 – Purac Biomaterials PLGA chemical structure. Adapted from [33].

The most widely used PLGA copolymers composition is 50:50 – ratio that identifies the PLGA polymers comprising 50% of both lactic and glycolic acid. Depending on the copolymer ratio and its molecular weight, the degradation time can range from a few months to years. For example, considering a PLGA polymer with more glycolic acid, which is more hydrophilic than the lactic acid, the degradation rate would be faster. This ability to modify the polymer's degradation rate conducts to another attractive characteristic of PLGA-based nanosystems that is the possibility of a sustained drug release and to tailor the release kinetics according to the pharmacokinetics of the encapsulated drug [29, 32].

Besides, there are other appealing properties which should not be forgotten, such as the possibility of targeting PLGA nanosystems to specific cells, tissues or organs, and of efficiently preventing drug degradation. Additionally, there is also the possibility of modifying PLGA nanosystems surface to provide both stealthness and a better interaction with biological tissues. Modifying surface properties such as its charge, by coating with PEG, chitosan or other hydrophilic polymers, can be an excellent way to improve their performance as drug delivery systems, since positively charged NPs establish ionic interactions with negatively charged cell membranes, facilitating cells interaction and uptake [29, 31].

PLGA NPs can be developed by a wide range of methods. One of the most common and preferred techniques is the emulsification-solvent evaporation technique, which allows the encapsulation of hydrophobic drugs. Briefly, it consists in dissolving the polymer and the drug in an organic solvent; the solvent is then evaporated and the NPs can be collected after centrifugation. However, this method does not fit for the encapsulation of hydrophilic drugs. Therefore, an update to this technique has been made, enabling hydrophilic drugs to be encapsulated in the PLGA NPs – the double emulsion. This method relies on dissolving the PLGA in an organic solvent and emulsion of an aqueous solution containing the hydrophilic drug within the organic phase. This primary emulsion is then transferred to an external aqueous solution containing a surfactant to stabilise the double emulsion, under vigorous stirring. In a similar manner, the organic solvent can be then evaporated and the NPs collected after centrifugation [29, 31, 32].

2.2. Superparamagnetic iron oxide nanoparticles for imaging

Magnetic resonance imaging (MRI) has been attracting major medical interest for early disease detection and staging. Indeed, MRI is one of the most used and effective tools for non-invasive clinical diagnosis. MRI images are acquired with high soft tissue contrast, and remarkable penetration depth and spatial resolution without the need to use any type of potentially harmful radiation that could cause undesired and damaging side-effects. In order to find better imaging for small and indistinct lesions and to provide better delimitation of diseased tissues, the scientific community is focused on MRI enhancement [34, 35].

Regarding magnetic materials, iron oxide is the one that is most investigated concerning applications in biomedical techniques such as the MRI, since it presents high biological compatibility. The design of a new strategy for MRI must fulfil some requirements, namely easy and economical synthesis, sufficient high magnetic moments, chemical stability in physiological conditions and low toxicity. Maghemite (γ - Fe_2O_3) and magnetite (Fe_3O_4) NPs are the best iron oxide examples of success in nanomedicine and nanotechnology industry [36-38].

Superparamagnetic iron oxide nanoparticles (SPIONs) are NPs with superparamagnetism – a phenomenon that occurs in magnetic materials when the particle core diameter is under 20 nm. FDA-approved SPIONs have been used in *in vivo* biomedical applications in different fields such as in tissue-specific release of therapeutic agents in cancer therapy and hyperthermia, among others. Having proved to be highly effective contrast agents for MRI diagnosis of solid tumours (Figure 5), the use of SPIONs as a contrast agent is among its most exciting applications [35-40].

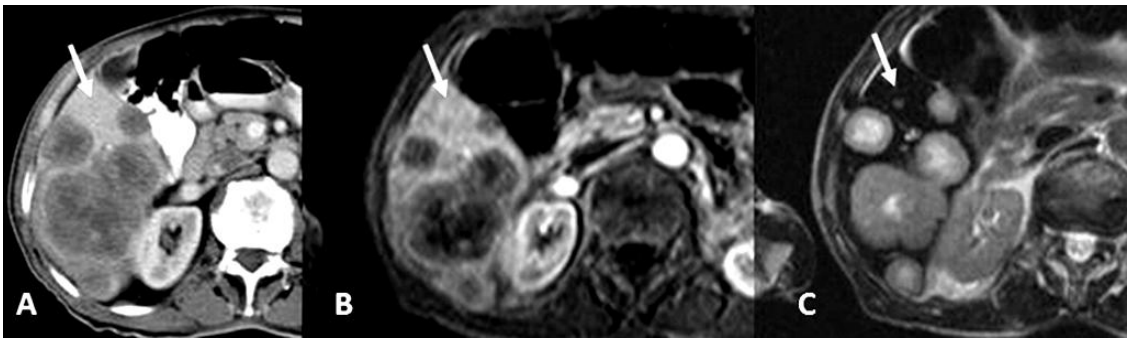

Figure 5 – Images of multiple liver metastases from colorectal carcinoma accessed by **(A)** computed tomography, **(B)** gadobenate dimeglumine-enhanced MRI and **(C)** SPIONs-enhanced MRI. Using SPIONs **(C)** it is possible to detect small lesions with much more higher contrast (arrow). Adapted from [40].

SPIONs present significant advantages when compared to the traditional contrast agents used in MRI and fulfil the aforementioned requirements for the strategy of finding a new contrast agent. These nanosystems present low cytotoxicity, longer lasting contrast enhancement and improved delineation of diseased tissues. Additionally, SPIONs can be simultaneously functionalised to provide: i) stealth regarding the immune system, ii) active targeting to a specific tissue and iii) efficient drug delivery, increasing local concentrations of SPIONS in the tissue of interest while decreasing the concentration in background tissues [34, 37, 38].

Most clinical preparations of SPIONs have been coated with dextran (*e.g.* Ferridex®, a sterile aqueous colloid of SPIONs associated with dextran used as a contrast agent for MRI) [41]. Another possible strategy, which attracts considerable attention for drug delivery, could be co-encapsulating SPIONs in polymeric NPs. The magnetic properties and the ease of functionalisation confer SPIONs a new purpose as theranostic agents – the use of SPIONs to significantly improve the actual means of simultaneous imaging and diagnosis [38, 42].

2.3. Antibody-conjugated nanoparticles

Immunoglobulins (Ig), commonly called antibodies, are a group of glycoproteins which are part of the specific immune system in vertebrate animals. Each antibody is composed by two large heavy chains and two small light chains linked by disulphur bridges, culminating on a peculiar Y-shaped protein (Figure 6). Depending on the heavy chain structure, immunoglobulins have different functions and can be divided in five different classes – IgG, IgE, IgD, IgA and IgM [43, 44].

Antibodies have two different domains: a carboxyl terminal (*Fc* region); and an amine terminal (*Fab* region) which comprises the antigen-binding domain and provides specificity and high affinity to antibodies. Taking into consideration these exclusive characteristics, antibodies have attracted great attention within the scientific community [43, 44].

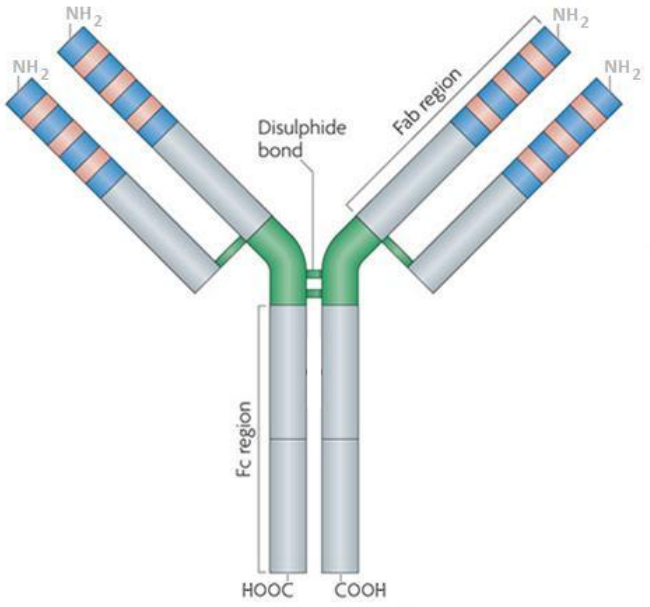

Figure 6 – Structure of an immunoglobulin. Adapted from [45].

A new trend of targeted drug delivery systems is emerging in nanomedicine. Numerous researchers are exploring new targeting moieties and respective receptors to achieve successful formulations. The basic principle behind ligand-targeted therapeutics is the association of molecules such as antibodies to the nanosystem. Hence, these ligands shall bind to target cells which receptors are either unique or overly expressed, when comparing to normal tissue cells [21, 46].

Since 1977, after Burstein and his colleagues demonstrated therapeutic action of an antibody linked to a cytotoxic drug in mice [47], several research groups have struggled to find more and better solutions using targeted drug delivery [44, 47-51]. A drug should be delivered to the desired tissue or organ safely, within the established dose and for the proper amount of time, in order to prevent or decrease systemic side effects. Besides, a targeted-system also improves the efficacy of the active molecule by increasing its distribution and concentration at the site of injury or disease [43, 48, 52].

There are already some examples of conjugation of NPs with antibodies, combining the remarkable properties of NPs such as their capability of working as drug carriers or intrinsic magnetic characteristics, with the targeting capacity of the latter. In 2007, Kocbek and her team tried two different approaches for NPs functionalisation, for recognition and specific targeting on breast epithelial cancer cell lines, through the use of antibodies [51]. Covalent and non-covalent binding were both applied to attach the antibody to the surface of polymeric NPs. The advantage of a covalent linkage compared to physical adsorption relies on the prevention of the competitive displacement of the adsorbed antibodies by blood components, hence increasing the nanosystem stability. However, in this attempt, only the non-covalent approach was successful [48, 51]. This obstacle was soon surmounted as later in the same year Scott and his colleagues successfully conjugated polymeric NPs with antibodies recognising the sigle-7 receptor, which is expressed on most acute myeloid leukaemias. Briefly, the group activated de NPs using a carbodiimide, forming a connecting amide bond through the conjugation of the antibody's primary amine group with the free carboxylic end group of the NPs [50].

Over the last few years, the number of publications regarding the integration of NPs and antibodies in targeted delivery has exponentially increased. However, antibody-conjugated NPs still face several challenges and hurdles until reaching the clinic, and to overcome them it is essential to conduct deeper and more comprehensive studies and research.

2.4. Targeted drug delivery to macrophages

The role of macrophages in numerous diseases, including cancer, atherosclerosis and infectious and inflammatory diseases, such as RA, is becoming better understood. Many approaches with surface-engineered nanocarriers-based targeting of macrophages are being investigated with both scientific and therapeutic interest. In an ideal targeted drug delivery strategy, the therapeutic efficacy of the drug would be maximised while its associated toxicity should be minimised [23, 53]. Macrophage-targeting approaches include the use of nanocarriers, such as liposomes, dendrimers, niosomes, carbon nanotubes, and also the celebrated NPs (Figure 7). Although not allowing for tissue-specific targeting due to its ubiquitous expression, mannose surges as a primary natural choice to target macrophages once it is expressed in the majority of macrophage populations [54].

In 2009, Nahar and his colleagues studied the macrophage mannose receptor using PLGA NPs. The purpose of their work was to develop a mannose-anchored nanosystem for efficient delivery of a polyene antifungal drug – amphotericin B – for visceral leishmaniasis treatment. The NPs showed enhanced macrophage uptake, suggesting a better targeting than using non-targeted nanosystems [45]. Although there is still room for improvement regarding targeted therapy, these results indicate that NPs can be a promising carrier for specific drug delivery to macrophages, in this specific case, using macrophage mannose receptor for effective treatment of visceral leishmaniasis [55, 56].

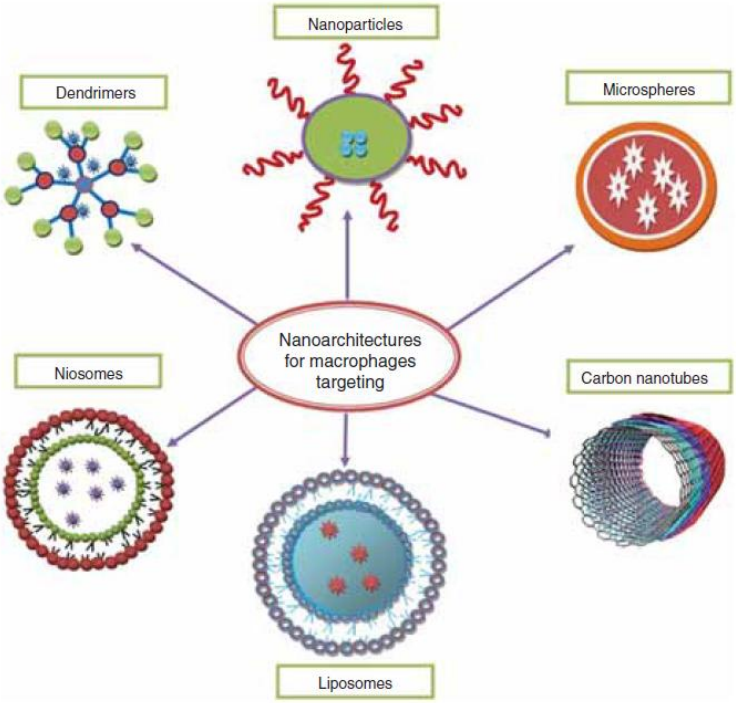

Figure 7 – Different nanocarriers used in macrophages targeting. Adapted from [53].

Regarding a different purpose, rifabutin, an antituberculosis drug, was loaded into solid lipid nanoparticles (SLN) before coating with mannose, for selective delivery to alveolar tissues. *Ex vivo* cellular uptake studies unveiled an almost six-fold enhanced uptake due to the mannose coating. Consequently, this approach supported the aforementioned strategies, confirming that the macrophage mannose receptor can be used for effective and targeted drug delivery to macrophages [57]. However, although this receptor is highly expressed on macrophages, it is not tissue-specific. Consequently, it does not constitute an ideal targeting strategy since NPs would target macrophages from several different tissues.

Being a localised disease, RA is a promising candidate to tissue-specific targeting strategies. RA inflammatory cells have overexpressed receptors which can work as potential targets to targeted drug delivery. Fueldner and colleagues found significant differences in the expression of the cellular receptors CD64, CD11b and CD304 in RA synovial tissue, providing suitable biomarkers to RA monitoring [58]. Other studies corroborate the former, proving that CD64 expression in normal joints is confined to the synovial lining cells, whereas in RA, it can be found that adding to the synovial lining, also in the sublining, perivascular space and stroma, CD64 expression levels are enhanced [59, 60].

CD64, also known as FcγRI (Fc-gama-receptor I), is a cell-surface receptor with high affinity for immunoglobulin G (IgG), especially IgG1. Hence, Vuuren and her team were pioneers using CD64-directed immunotoxins to target inflammatory macrophages from RA joints, taking advantage of the over-expression of CD64 [60, 61]. These emergent techniques make way to the potential use of the sensitive biomarker CD64 for RA screening, diagnosis or even treatment.

Currently there are no therapeutic strategies focusing directly on macrophages to treat RA. However, these recent results might encourage bolder approaches for its treatment. In fact, several research groups are struggling to find better solutions and to improve the already explored techniques.

In this work, we propose a pioneer approach for RA imaging and treatment through the use of SPIONs/PLGA NPs for macrophage-targeted delivery of MTX.

- This Page was intentionally left blank. -

3. Specific aims and strategy

In this work, an innovative approach for targeted therapy and imaging of RA was proposed. This study aimed at the development of a targeted theranostic system for intravenous administration, consisting on the encapsulation of both MTX, for RA therapy, and SPIONs, as MRI contrast imaging agent, into PLGA NPs. Thereafter, PLGA NPs were functionalised with a monoclonal antibody (mAb) against the macrophage specific cell surface receptor, CD64, which is overly expressed in RA (Figure 8).

The project was divided in a first phase, consisting of research, state of the art characterisation and definition of the work plan, performed during the first semester of the school year, from October until February. The second phase was accomplished from February until June, and consisted on the development of the research work, conducted at the Department of Chemical Sciences at the Faculty of Pharmacy, University of Porto.

Regarding the research work, preliminary studies were performed concerning PLGA NPs preparation. After the optimisation, four different formulations were produced, namely PLGA NPs, MTX-loaded PLGA NPs, SPIONS-loaded PLGA NPs and MTX- and SPIONs-loaded PLGA NPs, in order to access and compare final properties. Physicochemical properties of the developed NPs were extensively characterised to examine particle size, polydispersion, zeta potential and morphology, as well as to determine the MTX content, SPIONs encapsulation and antibody conjugation. The last task relied on *in vitro* studies, with the macrophage cell line RAW 264.7. These cells were cultured, and the developed PLGA NPs were tested assessing cell viability, NPs cytotoxicity and uptake.

This approach could bring a new insight for theranostic strategies, since targeted NPs are promising candidates for the future in medicine. With this nanosystem the release and action of the drug could be potentiated and controlled without injuring healthy tissues and organs, simultaneously providing a non-invasive and specific imaging tool for RA.

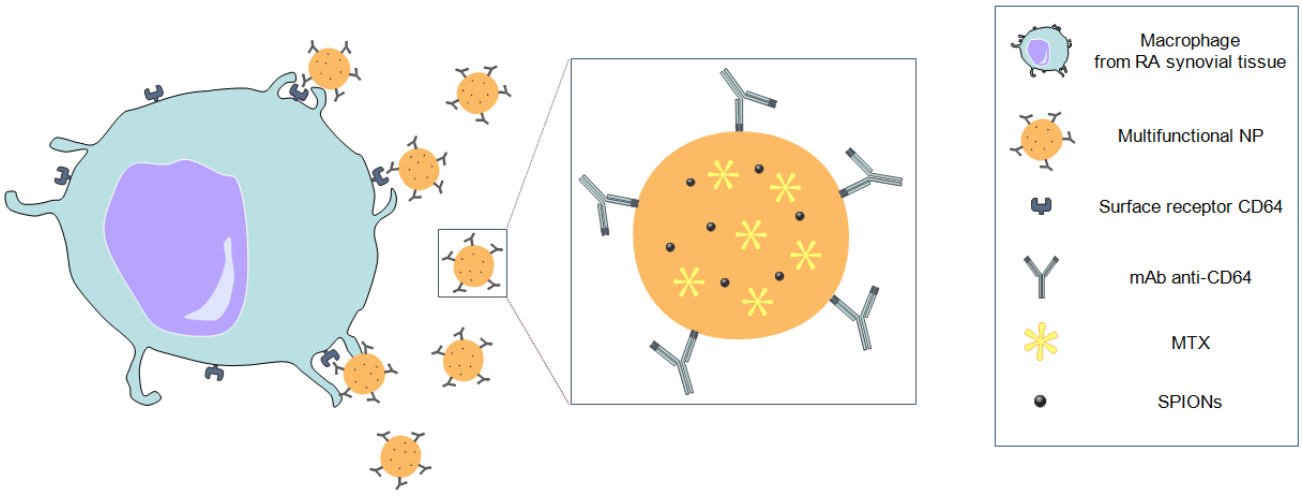

Figure 8 – Schematic of the proposed approach for targeted therapy and imaging of RA.

- This Page was intentionally left blank. -

4. Materials and methods

4.1. Materials

The polymers PLGA (50:50) PURASORB® PDLG 5002 and PURASORB® PDLG 5002A were a kind gift from Purac (Purac Biomaterials, Netherlands). MTX was obtained by courtesy of Excella (Excella GmbH, Germany). Maghemite NPs (15 nm) were kindly offered by Marcela Fernandes and her team (Chemical Department, Universidade Estudal Maringá, Brasil). Iron oxide nanocrystals (10 nm), with oleic acid coating and dispersed in chloroform (25 mg/mL), were gently provided by Ocean Nanotech Inc. (Arkansas, USA). Anti-Human CD64 (Fc gamma Receptor 1) antibody solution (1.0 mg/mL) was purchased from eBioscience (San Diego, California, USA). The Thermo-Scientific Pierce Micro BCA Protein Assay Kit was from Thermo Fisher Scientific (Rockford, IL, USA). LDH Cytotoxicity Detection Kit was from Takara Bio Inc. (Shiga, Japan). Poly(vynil alcohol) 87-90% hydrolysed and average Mw 30-70 kDa (PVA), dimethyl sulfoxide ACS reagent ≥99.9% (DMSO), dichloromethane (ACS reagent, ≥99.5% contains 50 ppm amylene as stabilize), ethyl acetate (ACS reagent, ≥99.5%), 2-morpholinoethanesulfonic acid low moisture content, ≥99% (MES), 1-ethyl-3-(3-dimethylaminopropyl) carbodiimide hydrochloride purum, ≥98.0% (EDC), N-hydroxysulfosuccinimide 98% (NHS), Thiazolyl Blue Tetrazolium Bromide 98% (MTT), Triton™ X-100 for molecular biology and Trypan Blue powder were purchased from Sigma-Aldrich (USA). Dulbecco's Modified Eagle's Medium (DMEM), Hanks' balanced salt solution (HBSS), Dulbecco's phosphate buffer saline 10x pH 7.4 (PBS), fetal bovine serum (FBS), Penicillin-Streptomycinm and Fungizone® Antimycotic were purchased from Gibco® (Invitrogen Corporation, UK).

4.2. Methods

4.2.1. Development of multifunctional NPs

4.2.1.1. Optimisation of NPs formulation

As the first attempt, PLGA (PURASORB® PDLG 5002 – ester terminated co-polymer) NPs were prepared using a solvent emulsification-evaporation method based on a w/o/w double emulsion technique. As standard procedure, 200 mg of PLGA were dissolved in 2 mL of dichloromethane, and 0.2 mL of Milli-Q water were added to the former. The solution was homogenised using a sonicator (VibraCell model VCX 130 equipped with a VC 18 probe, Sonics & Materials, Inc., Newtown, CT, USA), at 70% amplitude for 30 seconds. This primary emulsion was then added to 8 mL of 2% (w/v) PVA solution in Milli-Q water, and subsequently a second emulsion was completed by sonication in the same conditions. The homogenised solution was added to 15 mL of 2% (w/v) PVA solution in Milli-Q water under magnetic stirring and kept in these conditions overnight, until the organic solvent was fully evaporated. Regarding the NPs purification, the resulting solution was centrifuged (21,000 *g*, 10 minutes, 4ºC) and re-dispersed in Milli-Q water thrice for rinsing. The formulation was stored at 4ºC until further analysis [62].

To encapsulate SPIONs, 1 mg of maghemite NPs were added to the organic phase of the double emulsion (dichloromethane with PLGA) [63, 64]. Since SPIONs are magnetic NPs, the formulation could not be prepared under magnetic stirring, and this batch was prepared under mechanical stirring. However, after 24 hours, the organic solvent had not evaporated and dark large agglomerates were formed, most likely due to the low encapsulation of SPIONs using this technique. Additionally, MTX is practically insoluble in water [65], and the double emulsion technique demonstrated not to be the most appropriate method to efficiently encapsulate the drug. Therefore, this preparation method was further adapted in order to achieve an optimised approach. In the following preparation of nanoparticles, PLGA with carboxylic acid end groups was used in order to allow the binding of the anti-CD64 antibody to the NPs.

4.2.1.2. Preparation of NPs

Formulations containing the PLGA (PURASORB® PDLG 5002A – acid terminated co-polymer) were prepared using a solvent emulsification-evaporation method based on a w/o single emulsion technique. As standard procedure, 200 mg of PLGA were dissolved in 2 mL of ethyl acetate, and then added to 8 mL of 2% (w/v) PVA solution in Milli-Q water. The solution was homogenised using a sonicator (VibraCell model VCX 130 equipped with a VC 18 probe, Sonics & Materials, Inc., Newtown, CT, USA), at 70% amplitude for 30 seconds. This single emulsion was then added to a round-bottom flask with 15 mL of 0.2% (w/v) PVA solution in Milli-Q water. Regarding the organic solvent evaporation, a rotavapor was used for 1 hour and 30 minutes (300 hPa, 35ºC). Concerning the NPs purification, the resulting solution was centrifuged (21,000 *g*, 10 minutes, 4ºC), and re-dispersed in Milli-Q water thrice, for rinsing. The formulation was stored at 4ºC until further analysis.

To encapsulate MTX and SPIONs (Ocean Nanotech Inc.), both separate and simultaneously, the same methodology previously described was used. After dissolving 200 mg of PLGA in 2 mL of ethyl acetate, 20 mg of MTX or/and 40 µL of SPIONs dispersion (25 mg/mL in chloroform) were added, and the solution was homogenised using a vortex mixer (Figure 9).

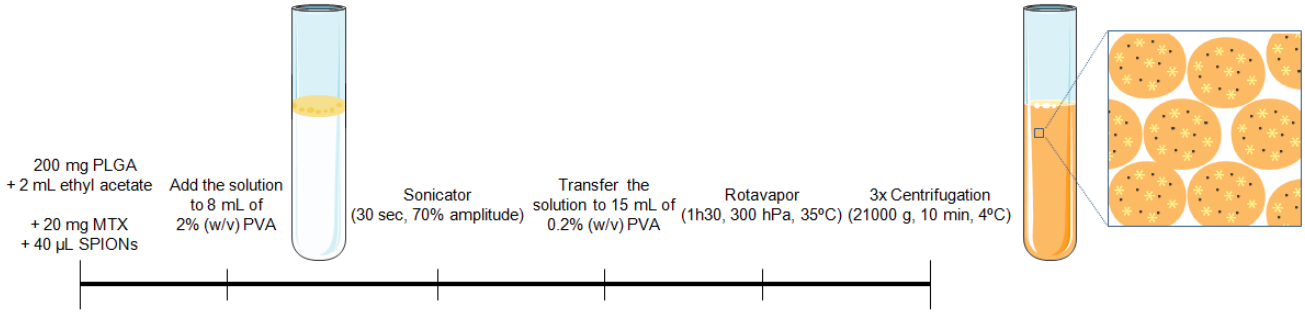

Figure 9 – Schematic of the preparation of multifunctional PLGA NPs.

4.2.1.3. Anti-CD64 conjugation of PLGA NPs

As previously mentioned, phagocytosis by macrophages can be initiated by Fc regions of IgG that bind to the Fc receptors in cells membrane. When a particle is coated or opsonised with an IgG, the Fc regions of the antibody bind to the corresponding receptors in the macrophage membrane and a phagocytic response is initiated [66]. Considering that CD64 is a FcγRI receptor, the anti-CD64 antibody should be linked through the Fab fragment, leaving the Fc region available for macrophages recognition. Therefore, the coupling reaction was carried out in the presence of EDC and NHS aiming for the NPs activation. The NPs will subsequently react with the primary amine of the antibody (Fab), yielding an amide bond, which allows the NPs functionalisation.

A volume of 11.5 mL of purified NPs (corresponding to 100 mg of PLGA) were centrifuged (21,000 *g*, 10 minutes, 4ºC) and re-dispersed in 10 mL of MES buffer, pH 5.0. The pH was maintained at 5.0 in order to maximise the attachment of EDC to the PLGA carboxylic acid groups. The activation was achieved by adding 1 mL of 0.1 M EDC and 1 mL of 0.7 M NHS (both dissolved in MES buffer, pH 5.0) to the NPs suspension, which was kept at room temperature for 1 hour, under moderate stirring. To remove the remaining reagents, the activated NPs were centrifuged (21,000 *g*, 10 minutes, 4ºC) and re-dispersed in PBS thrice, yielding a final concentration of 1.0 mg/mL. To conjugate the antibody to the activated PLGA NPs, 1 mL of the activated-NPs suspension was transferred to an Eppendorf® tube and 10 µL of the anti-CD64 antibody solution (1.0 mg/mL) were then added. After homogenising with a vortex mixer, the suspensions were incubated at 4ºC for 24h. The conjugated NPs were once again centrifuged at (30,000 *g*, 10 minutes, 4ºC), to remove the excess unconjugated antibody and reagents (Figure 10) [50].

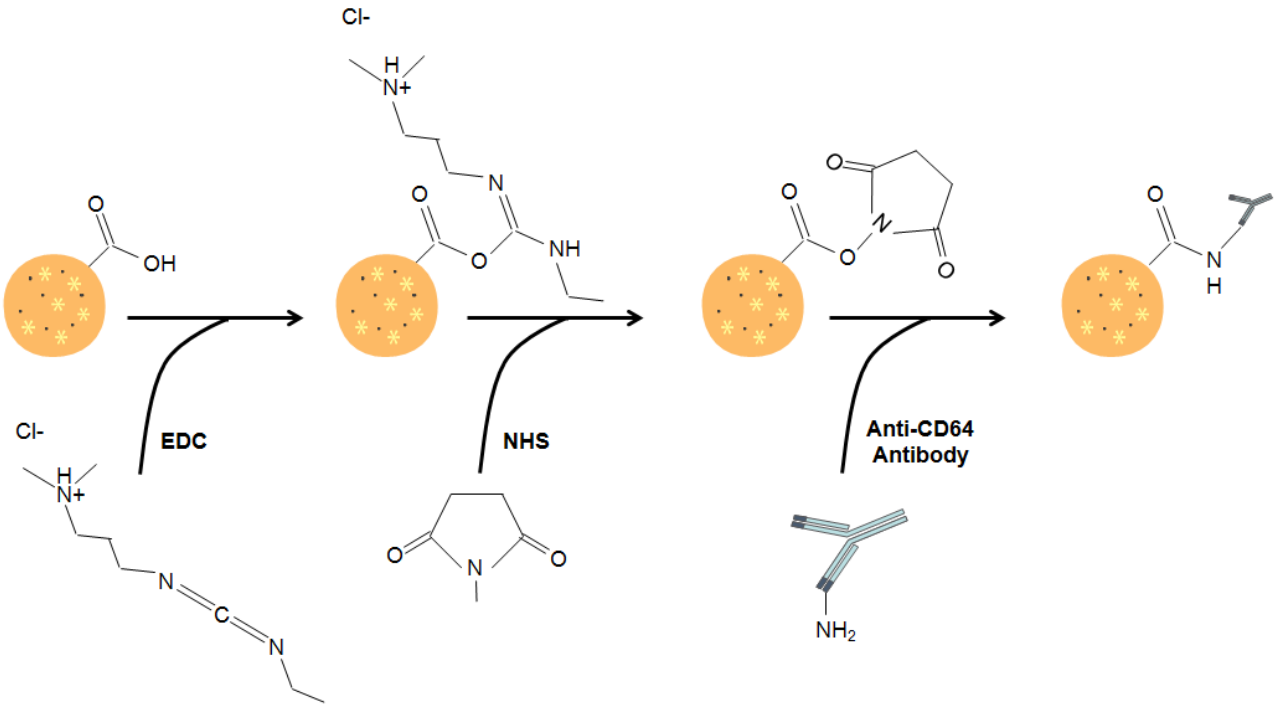

Figure 10 – Schematic of the functionalisation of multifunctional PLGA NPs with the anti-CD64 antibody.

4.2.1.4. Freeze-drying of the PLGA NPs

To freeze-dry the NPs, samples were poured into Eppendorf® tubes on a VirTis AdVantage 2.0 BenchTop Freeze Dryer (SP Scientific). The samples were frozen at -60ºC for 12 hours. A primary drying was performed at 20 ºC at 150 mTorr, for 20 hours. A secondary drying was also performed, at 25 ºC, 100 mTorr, for 20 hours, to complete sublimation. The condenser was maintained at -80ºC at 150 mTorr.

4.2.2. Nanoparticle characterisation

4.2.2.1. Dynamic light scattering and phase analysis light scattering

Dynamic Light Scattering (DLS), also known as Photon Correlation Spectroscopy, is a common technique for measuring the size of particles in the sub micron range. It measures Brownian motion of particles suspended within a liquid, through changes in the intensity of light scattered from particles through time. Consequently, the slower the motion the larger the particle will be, since smaller particles are more affected by interactions with the solvent. Considering this motion, and the temperature and viscosity of the sample throughout the analysis, DLS can calculate the hydrodynamic diameter of the particle [67].

The zeta potential is a physical property which is exhibited by all particles in suspension. It is an important parameter in understanding the electric double layer repulsion and it can be measured by phase analysis light scattering. When an electric field is applied across an electrolyte, charged particles in suspension are attracted towards the electrode of opposite charge while viscous forces acting on the particles tend to oppose the movement. When equilibrium is reached, the particles move with constant velocity, also known as electrophoretic mobility, and the zeta potential can be measured. The magnitude of the zeta potential gives an indication of the potential stability of the system. If the modulus of the zeta potential is large, the particles in suspension will tend to repel each other. Hence, there will be no tendency to agglomerate. Contrastingly, when zeta potential values are low, it means that there will be no force to prevent the particles coming together and agglomerate [68].

The produced NPs were characterised by means of particle size, size distribution (polydispersity index), and zeta potential. Mean diameter and polydispersity index were assessed by DLS using a 90Plus Particle Size Analyzer (Brookhaven Instruments Corporation) and the zeta potential was determined by phase analysis light scattering using a ZetaPALS Zeta Potential Analyzer (Brookhaven Instruments Corporation), at 660 nm, with a detection angle of 90°, at 25ºC. The samples were diluted to a suitable concentration: 20 µL of non-conjugated NP dispersion (4 mg/mL) to 1580 µL of Milli-Q water, and 80 µL of antibody-conjugated NP dispersion (1 mg/mL) to 1520 µL of Milli-Q water. All measurements were performed with six repetitions, for each of the three independent batches of NPs.

4.2.2.2. Scanning electron microscopy

Scanning electron microscopy (SEM) is based on the incidence of a beam of accelerated electrons on the sample. These accelerated electrons interact with the sample, exciting its atoms which emit secondary electrons. According to the angle between the primary beam and the surface of the sample, it is possible to detect and analyse the surface topography.

In order to evaluate the morphology of the developed NPs, SEM was performed using a High Resolution Quanta™ 400 Scanning Electron Microscope (FEI™). Samples were prepared by two different methods: 1) samples of NP dispersion were mounted on metal stubs and air-dried; 2) samples of NP dispersion were freeze-dried and only then mounted on conductive carbon adhesive tabs, on metal stubs. Subsequently, they were coated with a gold/palladium thin film by sputtering for 60 seconds, with a 15 mA current, using a SPI Module Sputter Coater system.

4.2.2.3. Transmission electron microscopy

Unlike SEM, transmission electron microscopy (TEM), which is also based on the incidence of an accelerated beam of electrons to the sample, is not a surface analysis technique. In TEM, thin samples (less than 0.5 µm) are illuminated by the electron beam, and the image is recorded by detecting the electrons that pass through the sample into a system of electromagnetic lenses which focus and enlarge the image.

Each NP formulation sample was prepared by placing 10 µL of NP dispersion on a copper-mesh grid, after 2 minutes, excess water was removed by touching with filter paper. For contrasting, 10 µL of 0.75% uranyl acetate solution were added and let at room temperature, for 30 seconds. The grids were then observed in a JEM-1400 Transmission Electron Microscope (JEOL Ltd.), with an accelerating voltage of 80 kV.

4.2.2.4. High Performance Liquid Chromatography

High Performance Liquid Chromatography (HPLC) is a chromatographic technique used to separate individual components of a mixture, based on their hydrophobicity, thus enabling their identification and quantification. This technique was used to determine the association efficiency of MTX in the developed MTX-loaded PLGA nanosystems.

To separate MTX from other substances, a specific method had to be adapted [69, 70]. MTX quantification was performed using a Merck-Hitachi LaChrom HPLC System at room temperature, equipped with a reversed-phase symmetry column (25 cm length x 4.6 mm internal diameter; 5 µm particle size; Waters Corporation, Milford, MA, USA) in conjunction with a pre-column C18 insert. The mobile phase was composed by 60:40 (v/v) water/acetonitrile, in an isocratic system, at a flow rate of 1 mL/min. The wavelength was set for 313 nm, and the 20 µL injection loop autosampler was used. Standard MTX solutions were prepared at final concentrations of 1, 3, 6, 10, 25, 50 and 100 µg/mL in Milli-Q water, in order to obtain a standard linear curve for HPLC analysis (Figure 11).

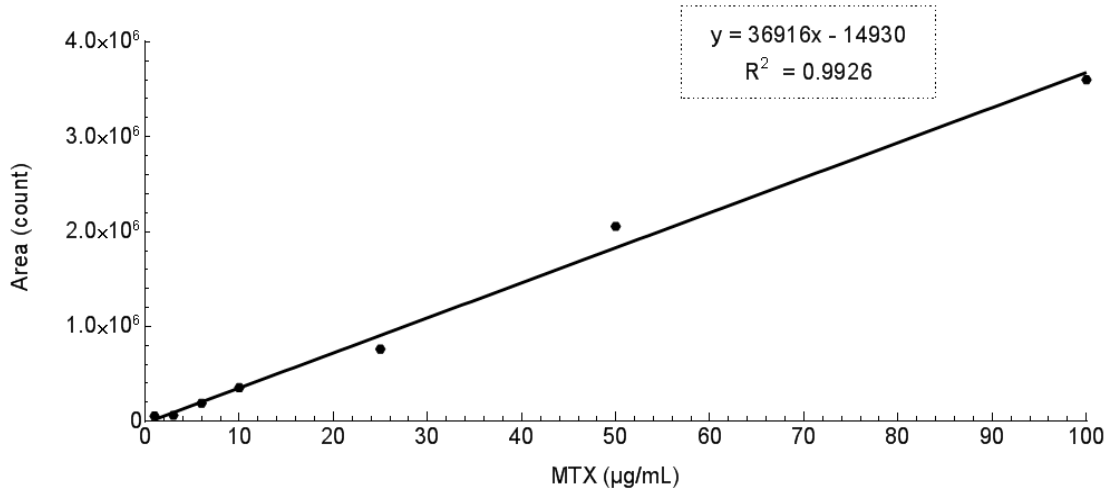

Figure 11 – Standard curve for MTX quantification using HPLC.

The samples correspond to 500 µL of the supernatant of the first centrifugation during NPs purification of MTX-loaded NPs and MTX and SPIONs-loaded NPs, from all three replicates. Before doing the analysis, samples were centrifuged (30,000 *g*, 10 minutes, 4ºC) to eliminate NPs that eventually remained in the supernatant. Subsequently, the quantification of the compound was carried out by measuring the peak areas in relation to the standards. The association efficiency of MTX was determined indirectly by subtracting the amount of MTX that remained in the aqueous phase to the total amount of MTX used to prepare the NPs (20 mg of MTX to 23 mL of final formulation) (Equation 1).

$$(1) \quad \text{Association Efficiency (\%)} = \frac{\text{Total amount of MTX} - \text{Free MTX in supernatant}}{\text{Total amount of MTX}} \text{x100}$$

4.2.2.5. Fourier Transform Infrared Spectroscopy

Fourier Transform Infrared (FT-IR) spectroscopy is an advanced technique which relies on an infrared beam to collect an absorbance/transmittance spectrum of the vibrations of chemical bonds in function of wavelength, allowing the identification of a sample's components. Regarding the need to ascertain both drug encapsulation and antibody conjugation, FT-IR spectroscopy proved to be an invaluable technique to confirm unequivocally the presence of both components and the efficacy of the previously described procedures to develop the projected multifunctional NPs.

The developed NPs were characterised by FT-IR analysis, using a Frontier FT-IR Spectrometer with Universal ATR Sampling Accessory (PerkinElmer, USA). NPs were lyophilised as described before, and for each spectrum a 50-scan was collected with 4 cm^{-1} resolution in the mid-infrared region (3600 to 600 cm^{-1}).

4.2.2.6. Antibody quantification

The amount of antibody conjugated to NPs was evaluated by quantifying protein attached to the surface of NPs from each formulation. The Thermo-Scientific Micro BCA Assay Kit is a detergent-compatible bicinchoninic acid (BCA) formulation for the colorimetric detection and quantification of total protein. The method utilises BCA as the detection reagent for Cu^{+}, which is formed when Cu^{2+} is reduced by protein in an alkaline environment. A purple-coloured reaction product is formed by the chelation of two molecules of BCA with a cuprous ion (Cu^{1+}). This water-soluble complex exhibits strong absorbance at 562 nm which increases linearly with increasing protein concentrations [71].

Briefly, diluted bovine serum albumin (BSA) standards were prepared (40, 20, 10, 5, 2.5, 1, 0.5 µg/mL) using a diluent equal to the sample buffer, PBS. Afterwards, the Micro BCA working reagent was prepared according to the instructions. The microplate procedure was performed: 150 µL of each standard or unknown sample were pipetted to a 96-well microplate, and 150 µL of BCA working reagent were added to each well. The microplate was mixed thoroughly for 30 seconds, and then covered and incubated for 2 hours, at 37ºC. After the incubation time, the plate was cooled to room temperature and the absorbance was read at 562 nm on a microplate reader (Synergy™ HT Multi-mode Microplate Reader, BioTek Instruments, USA). The average 562 nm reading of the Blank standard replicates were subtracted from the 562 nm reading of all individual standards and unknown sample replicates. A standard curve was computed, plotting the average Blank-corrected 562 nm reading for each BSA standard versus its corresponding concentration in µg/mL (Figure 12). The protein concentration of each unknown sample was determined using the standard curve [50, 71].

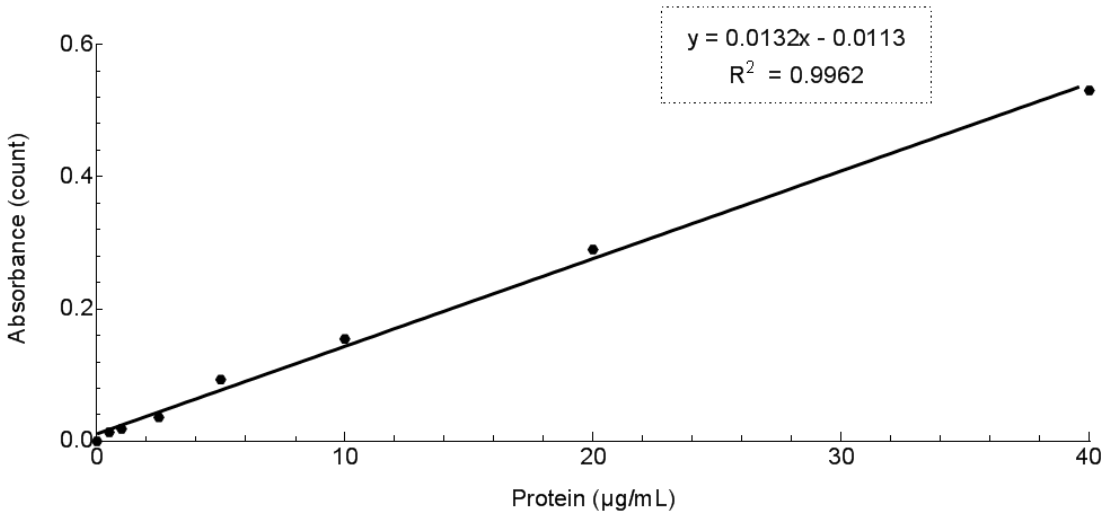

Figure 12 – Standard curve for protein quantification using the BCA Assay Kit.

4.2.3. *In vitro* studies

4.2.3.1. Cell culture

RAW 264.7 (ATTC® TIB-71™) cells (passage 31-38) were culture in DMEM medium supplemented with 10% FBS, 1% Penicillin-Streptomycin and 1% Fungizone® Antimycotic, and maintained in a humidified incubator at 37ºC, under a 5% CO2 atmosphere. Medium was changed every two or three days. For sub-culturing, cells were detached by scrapping, and counted in a Neubauer chamber diluted in a Trypan Blue solution 0.4% (w/v) in HBSS to exclude non-viable cells. For 75 cm^2 flasks, appropriate aliquots of the cell suspension were plated with a sub-cultivation ratio of 1:3. The volume of culture medium was adjusted for a new culture flask [72].

4.2.3.2. MTT assay

The MTT assay is a colorimetric assay used to access cell metabolism in growth and proliferation, measuring the activity of cellular enzymes that reduce the thiazolyl blue tetrazolium bromide (MTT) substrate, to formazan, resulting on a dark purple colour [73]. Before performing the assay, a standard curve must be designed, to know the most suitable cell seeding concentration for the measurements to fall into the assay linear detection range. Therefore, 200 µL of cell suspension at different cell concentrations (1000, 5000, 10000, 15000, 20000, 40000, 50000, 80000 and 100000 cells/mL) were seeded into wells of 96-well tissue culture test plates (Orange Scientific products, Belgium). After 24h of culturing on a humidified incubator at 37ºC under a 5% CO2 atmosphere, the culture medium was removed and 200 µL of fresh warm medium were added. 24 hours later the medium was removed, 200 µL of MTT solution (5 mg/mL MTT in HBSS) were added to the cultures, diluted to a final concentration of 0.5 mg/mL in culture medium, and the plate was incubated for 4 hours at 37ºC, in the dark. The MTT solution was discarded and 200 µL of DMSO were added, to solubilise the formazan crystals formed by the MTT reaction. The plate was shaken for 10 minutes, at room temperature, under light protection. The absorbance was measured using a microplate reader (Synergy™ HT Multi-mode Microplate Reader, BioTek Instruments, USA) at 590 nm and 630 nm for background subtraction. The results, from three experiments for each cell density, were analysed by plotting absorbance versus cell seeding density (Figure 13), and the right density, $2.5x10^4$ cells/mL, was chosen according to the value registered in the middle of the linear curve [73].

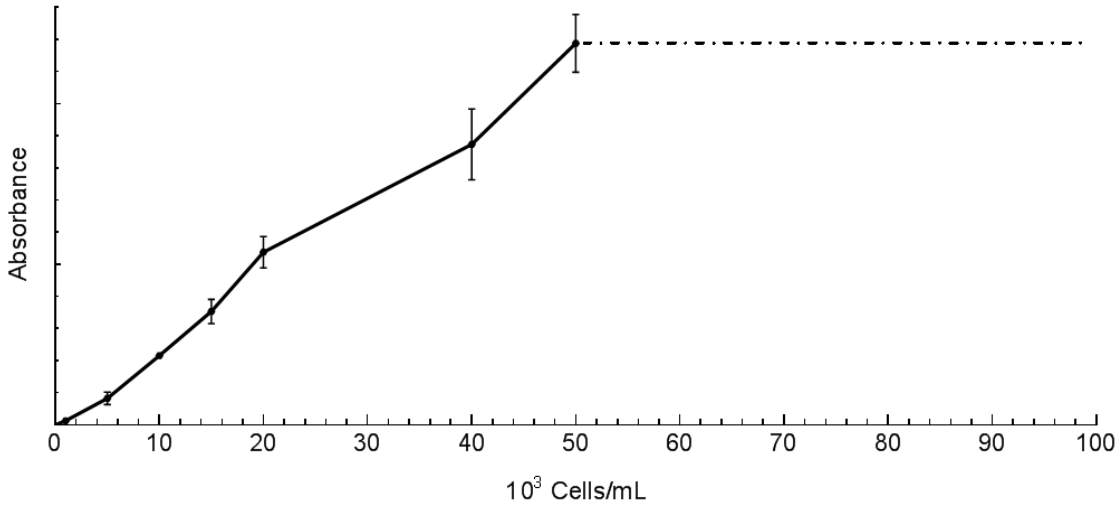

Figure 13 – Standard Curve for cell seeding density on MTT assay. The density chosen was $2.5x10^4$ cells/mL which falls in the middle of the linear range of detection of the assay. Values over $5.0x10^4$ cells/mL resulted in either substrate saturation or cell death.

After determining the appropriate cell seeding density for this assay, MTT assay was performed with the developed NPs, at different concentrations, on RAW 264.7 cells. 200 µL of cell suspension ($2.5x10^4$ cells/mL) were seeded into wells of 96-well tissue culture test plates (Orange Scientific products, Belgium). After 24h of seeding on a humidified incubator at 37ºC under a 5% CO2 atmosphere, the culture medium was removed and 200 µL of NP dispersion were added with different concentrations (0.1, 1, 10, 100 and 1000 µg/mL). A positive control (200 µL of culture medium) and a negative control (200 µL of Triton™ X-100 2% (w/v) in culture medium) should be included, in order to normalise the results. After 24 hours of incubation with the NPs, the MTT assay was performed as previously described. Cell viability was determined according to the following equation:

$$(2) \quad \text{Viability (\%)} = \frac{\text{Experimental Value} - \text{Negative Control}}{\text{Positive Control} - \text{Negative Control}} x100$$

4.2.3.3. LDH assay

Lactate dehydrogenase (LDH) is a cytoplasmatic enzyme which is present in most cells. Once the cytoplasmic membrane is damaged, this enzyme is released to the cell culture medium and consequently can be quantified by the LDH Cytotoxicity Detection Kit, allowing the assessment of cell death. The cell culture supernatant is collected and, after incubation with the kit reaction mixture, the formazan formed is measured. An increase in the number of dead or plasma membrane-damaged cells leads to an increase of the LDH enzyme activity in the culture medium, which can be directly correlated to the amount of formazan formed [74].

The viability and the cytotoxicity assays have several steps in common, namely cell seeding into wells of 96-well tissue culture test plates, 24 hours of incubation at 37ºC under a 5% CO2 atmosphere and NP dispersion addition with different concentrations. After the second incubation of 24 hours, on the MTT assay the medium should be removed and discarded; contrarily, what is crucial for the LDH assay is the collection of the culture medium after the incubation. Hence, the supernatant of the MTT assay was removed and transferred to other 96-well tissue culture test plates (Orange Scientific products, Belgium) and the LDH assay proceeded. The collected cell culture medium was centrifuged (250 *g*, 10 minutes, room temperature). Carefully, without disturbing the pellet, 100 µL were removed from each well and were transferred into the corresponding wells of new 96-well tissue culture test plates. 100 µL of the LDH Cytotoxicity Detection Kit reaction mixture were added, and the plates were incubated 30 minutes at room temperature, protected from light. The absorbance was measured using a microplate reader (Synergy™ HT Multi-mode Microplate Reader, BioTek Instruments, USA) at 490 nm and 630 nm for background subtraction [74]. Nanoparticles' cytotoxicity was determined according to the following equation, bearing in mind, that this being a cytotoxicity assay, the negative control are now the untreated cells and the positive control are now the cells treated with the 2% Triton X-100 solution:

$$(3) \quad \text{Cytotoxicity (\%)} = \frac{\text{Experimental Value} - \text{Negative Control}}{\text{Positive Control} - \text{Negative Control}} \times 100$$

4.2.3.4. Uptake studies

Intracellular and cell associated drug levels of MTX were assessed by quantifying the amount of drug associated with RAW 264.7, after incubation with functionalised and non-functionalised NPs or free MTX dispersed in culture medium at a pre-defined concentration and at different time points. Briefly, 2 mL of cell suspension (1.5×10^5 cells/mL) were seeded into wells of 6-well tissue culture test plates (Orange Scientific products, Belgium). After 24 hours of culturing on a humidified incubator at 37ºC under a 5% CO2 atmosphere, the culture medium was removed and the wells were washed with 1 mL of HBSS, in order to remove unattached cells and/or cellular debris. 2 mL of NPs and MTX dispersion in culture medium, with a final correspondent concentration of MTX equal to 1 µg/mL, were added to the wells. The plates were incubated for different amounts of time (15, 30, 60, 120, 240 and 360 minutes) at 37ºC under a 5% CO2 atmosphere. For each time point, the culture medium was removed, and the cells were washed thrice with HBSS, in order to remove extracellular drug or NPs. 400 µL of Triton™ X-100 solution (2% w/v in PBS) were added to each well, and the plates were let at 4ºC for 30 minutes, for cell lysis. Cell lysates were collected to Eppendorf® tubes, and centrifuged (30,000 *g*, 10 minutes, 4ºC).

After centrifugation, the supernatant was collected to different Eppendorf® tubes, and the amount of soluble protein was assessed with the Thermo Scientific Pierce BCA Kit. The remaining supernatant samples were frozen until further processing. To quantify the intracellular and cell associated drug, HPLC was used. The supernatant was thawed, and 200 µl were collected and mixed with 400 µl of acetonitrile, in order to precipitate protein content and solubilise MTX possibly entrapped in NPs. The Eppendorf® tubes were, once more, centrifuged (30000 *g*, 10 minutes, 4ºC), and the supernatant was collected as described before [75]. The amount of MTX was finally determined by HPLC.

4.2.4. Statistical analysis

Statistical analyses were performed with IBM® SPSS® Statistics (SPSS 21.0, USA). Results are reported as mean ± standard deviation (SD) from a minimum of three independent experiments. Two-tailed Student's t-test and one-way analysis of variance (ANOVA) were performed to compare two or multiple independent groups, respectively. When the group was significantly different ($p<0.01$), differences between groups were compared within a post-hoc test (Tukey). Paired samples were analysed with the paired-samples two-tailed Student's t-test. Differences were considered significant at $p<0.01$.

- This Page was intentionally left blank. -

5. Results and discussion

5.1. Nanoparticle characterisation

For a successful RA-targeted theranostics approach, it is paramount that all components comprised in the devised PLGA nanoparticles, namely the SPIONs (for imaging diagnosis), the MTX (therapeutic drug) and the anti-CD64 antibody (for specific RA-macrophage targeting), are effectively integrated in the NP, without altering significantly their renowned drug delivery features.

The first indication of the successful conjugation of all these agents was the visual confirmation that all the four formulations, prior to antibody conjugation, presented different colour and aspect after extensive rinsing of the exceeding reagents in solution (Figure 14). This elicited the initial proof that SPIONs and MTX were both, separate and simultaneously, incorporated into the PLGA NPs, which was possible to detect with the naked eye.

The developed NPs were devised aiming at an intravenous administration strategy for RA targeted therapy and imaging. Therefore, the physicochemical properties of the developed NPs, which influence their physical stability and future interaction with cells and biological tissues, must be regarded with utmost importance. Further and more extensive characterization of the NPs, in terms of their particle size and polydispersity index (PdI), zeta potential, SPIONS and MTX encapsulation, and antibody functionalisation, is addressed in the following chapters. Table 1 summarises the main features assessed for all the disparate PLGA NP formulations produced.

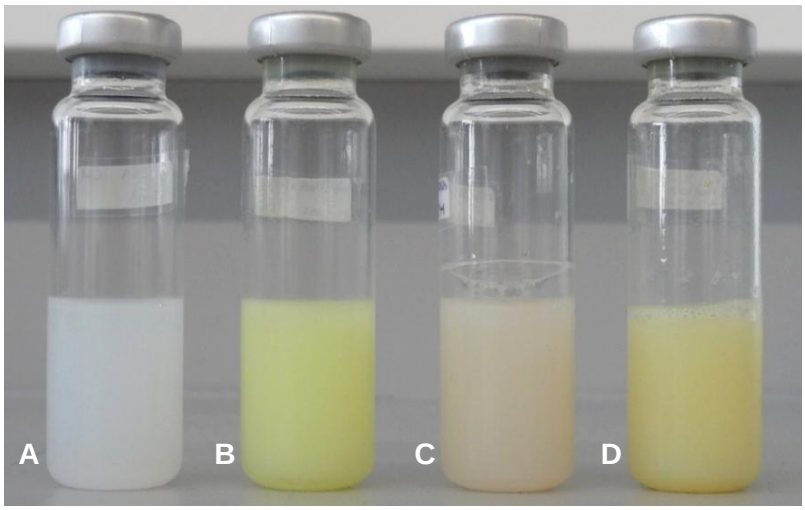

Figure 14 – Multifunctional PLGA NPs developed by a solvent emulsification-evaporation method based on a w/o single emulsion technique: **(A)** PLGA NPs, **(B)** MTX-loaded PLGA NPs, **(C)** SPIONs-loaded PLGA NPs and **(D)** MTX- and SPIONs-loaded PLGA NPs.

Table 1 – Physicochemical properties of the developed multifunctional PLGA NPs. Mean effective diameter, PdI and zeta potential of all formulations; MTX association efficiency of MTX-loaded PLGA NPs before functionalisation; anti-CD64/NPs ratio and anti-CD64 conjugation efficiency of functionalised PLGA NPs.

Formulation	Mean Effective Diameter (nm)	PdI	Zeta Potential (mV)	MTX Association Effiency (%)	Anti-CD64/NPs Ratio (µg/mg)	Anti-CD64 Conjugation Efficiency (%)
PLGA NPs	140.7 ± 17.8	0.21 ± 0.10	-29.4 ± 5.5	-	-	-
PLGA NPs + MTX	136.5 ± 6.9	0.23 ± 0.10	-27.3 ± 4.4	98.0 ± 0.4	-	-
PLGA NPs + SPIONs	131.3 ± 11.5	0.22 ± 0.04	-25.2 ± 5.0	-	-	-
PLGA NPs + MTX and SPIONs	157.4 ± 21.5	0.11 ± 0.10	-32.5 ± 4.6	94.9 ± 1.6	-	-
PLGA NPs + Anti-CD64	168.6 ± 14.7 [c]	0.24 ± 0.05 [c]	-18.0 ± 4.3 [c]	-	2.69 ± 1.21	26.9 ± 12.1
PLGA NPs + MTX + Anti-CD64	162.0 ± 23.9 [c]	0.25 ± 0.11 [c]	-16.4 ± 3.2 [c]	-	1.65 ± 0.5	16.5 ± 5.0
PLGA NPs + SPIONs + Anti-CD64	192.2 ± 12.0 [b, c]	0.15 ± 0.06 [b, c]	-19.3 ± 3.0 [b, c]	-	1.39 ± 1.05	13.9 ± 10.5
PLGA NPs + MTX and SPIONs + Anti-CD64	202.0 ± 9.5 [b, c]	0.34 ± 0.02 [b, c]	-21.1 ± 2.2 [b, c]	-	2.98 ± 0.46	29.8 ± 4.6

Values represent mean ± SD (n ≥ 3).
a - Significantly different ($p<0.01$) from PLGA NPs, between non-conjugated formulations.
b - Significantly different ($p<0.01$) from PLGA NPs, between conjugated formulations.
c - Significantly different ($p<0.01$) before and after functionalisation.

5.1.1. Particle size and zeta potential

It has been thoroughly described in previous publications that PLGA nanoparticles prepared by the simple emulsion technique should present a hydrodynamic diameter within the range of 100 to 250 nm [27, 29]. In order to avoid NPs sequestration by spleen sinusoids and liver *fenestræ*, the size of the nanosystem cannot be larger than 200 nm. In addition, NPs should not be smaller than 70 nm since particles with this size may penetrate capillary vessels. Subsequently, for a long circulation time, NPs size for intravenous administration should be between 70 and 200 nm [76, 77]. Indeed, all formulations tested in this work fell into sizes which range from approximately 135 nm for up to 200 nm (Table 1), supporting the anticipated results for this technique, even when in combination with MTX and SPIONS encapsulation and antibody conjugation.

Focusing now on the NPs non-conjugated with anti-CD64, both SPIONs and MTX encapsulation did not significantly affect particle size in all formulations, indicating that they probably do not considerably interfere with the NP formation by simple emulsion, and that it is possible to create a complex multi-functional NP while maintaining primary PLGA NPs qualities. Still concerning size, the PdI of these NPs was, at all instances, well below the reference level of 0.3 indicating that well-defined and mono-disperse NP populations were formed with uniform and consistent sizes without undergoing agglomeration.

Regarding particle charge, all tested formulations showed markedly negative zeta potential values (Table 1). A negative charge is typical of carboxyl-terminated NPs owing to the contribution of the –COOH groups which are deprotonated at physiological pH or, in this particular case, at the pH of Milli-Q water [51]. Although negatively charged nanoparticles may face higher difficulties when considering cellular uptake, due to electrostatic repulsion from cellular membranes, zeta potential values rounding -30 mV contribute to particle stability in solution avoiding the formation of agglomerates and thus stabilising particle size. Additionally, negative NPs present advantages over their cationic counterparts, as they are expected to be less cytotoxic, as for cationic NPs there is the risk of causing cell lysis by disrupting their membrane [29, 78]. Taking into consideration cellular uptake, further functionalisation of the NPs with a hydrophilic polymer such as chitosan or PEG can be a possibility for future work envisioning facilitated cell interaction.

Not surprisingly, zeta potential values significantly decreased in all formulations after conjugation with the anti-CD64 antibody (Table 1). The principle behind the antibody conjugation relies on the establishment of a covalent amide bond between the amine and carboxyl termini of the antibody and PLGA, respectively [49]. Consequently, a partial surface charge shielding will occur being related to the amount of carboxyl groups involved in the reaction with the amine termini of the antibody. Indeed, one can observe that the reduction in surface charge is in the same value range as the antibody conjugation efficiencies. Added to zeta potential, antibody conjugation interfered in particle size as well. NPs suffered a mean particle size shift in the order of the 30 to 50 nm (Table 1), which is justified by the presence of the antibody on the surface of the particles as well as by a higher water content on the hydration of the conjugate [49]. The particle size and zeta potential results suggest that the developed multifunctional PLGA NPs are promising candidates for a theranostic approach.

5.1.2. Scanning electron microscopy

SEM allowed learning information on the surface morphology of the NPs. SEM samples were initially freeze-dried prior to analyses. However, lyophilisation resulted in sample destruction and the NPs appeared as a degraded and fused polymer mass on top of the metal support (results not shown). Exception to the rule, anti-CD64-functionalised NPs were not degraded by the process up to the same extent (Figure 15 – E, F, G and H), indicating that the proteic antibody may have worked as a cryo-protectant during lyophilisation, although some particle fusion was visible. The other NPs (non-conjugated) were analysed as air-dried NP dispersions (Figure 15 – A, B, C and D). Further attempts should be made to standardise the sample preparation procedure to both NP categories. Nevertheless, SEM analysis shows the spherical shape of the NPs as well as their smooth surface, bereft of pores. The micrographs show NPs with sizes below 200 nm, supporting the previously obtained results (Table 1). The homogenous and flat surface, unvarying between one another, may suggest that both MTX and SPIONs are entrapped within the PLGA polymeric matrix, in detriment of the particles' surface.

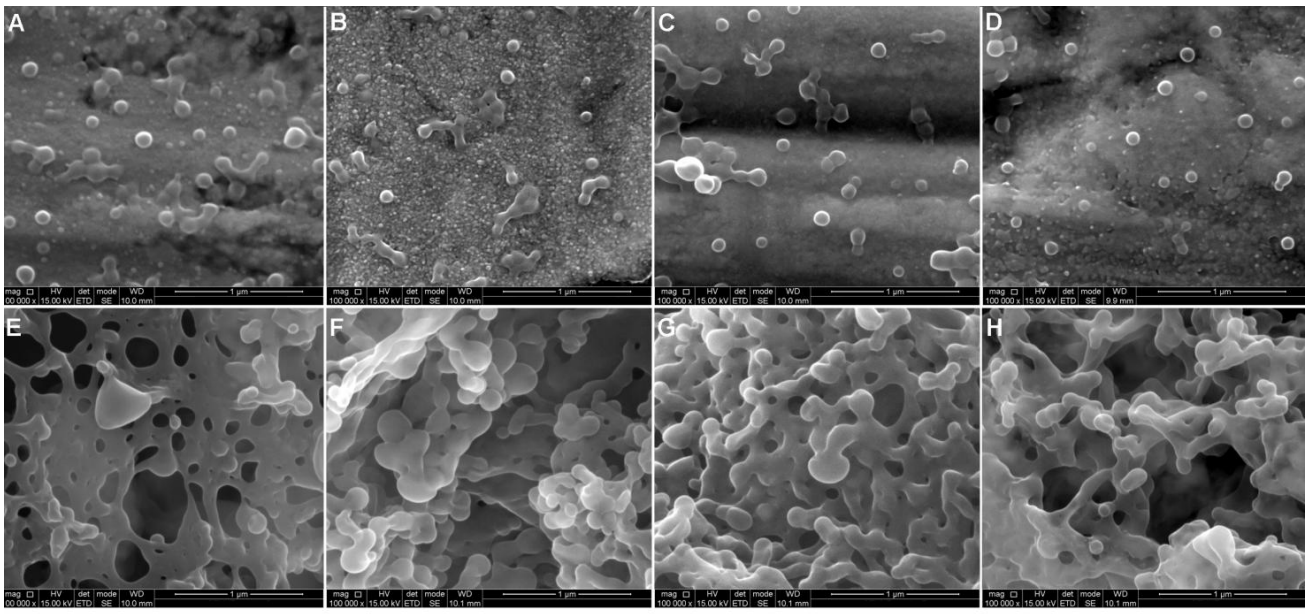

Figure 15 – Scanning electron micrographs of **(A)** PLGA NPs, **(B)** MTX-loaded PLGA NPs, **(C)** SPIONs-loaded PLGA NPs, **(D)** MTX- and SPIONs-loaded PLGA NPs**, (E)** anti-CD64-functionalised PLGA NPs, **(F)** anti-CD64-functionalised MTX-loaded PLGA NPs, **(G)** anti-CD64-functionalised SPIONs-loaded PLGA NPs, **(H)** anti-CD64-functionalised MTX- and SPIONs-loaded PLGA. Scale bars correspond to 1 µm. Magnification 100,000 x.

5.1.3. Transmission electron microscopy

TEM allowed an easy confirmation of the results obtained by DLS on particle size. The micrographs (Figure 16 and Figure 17) show a mono-disperse population of isolated, smooth and spherical particles with well-defined sizes, which were at all times well below 200 nm, corroborating the previously obtained results of NP characterisation. One can also affirm that MTX and SPIONs encapsulation, as well as antibody conjugation, did not considerably affect particle shape and overall size.

Figure 16 (C1 and C2) and Figure 17 (G1 and G2) show SPIONs-encapsulated NPs in which SPIONs are evident in a considerable number inside the PLGA NPs as smaller and electronically denser well-dispersed spots, confirming their efficient encapsulation both alone and when co-encapsulated with MTX (Figure 16 (D1 and D2) and Figure 17 (H1 and H2)). Regarding the antibody conjugation, Figure 17 shows micrographs of the NP formulation after conjugation with the anti-CD64 antibody and one can often see a denser and thicker ‘corona’ (red arrow head) surrounding the lighter NP core which may indicate the presence of the antibody either adsorbed or covalently linked to the surface of the NP [79].

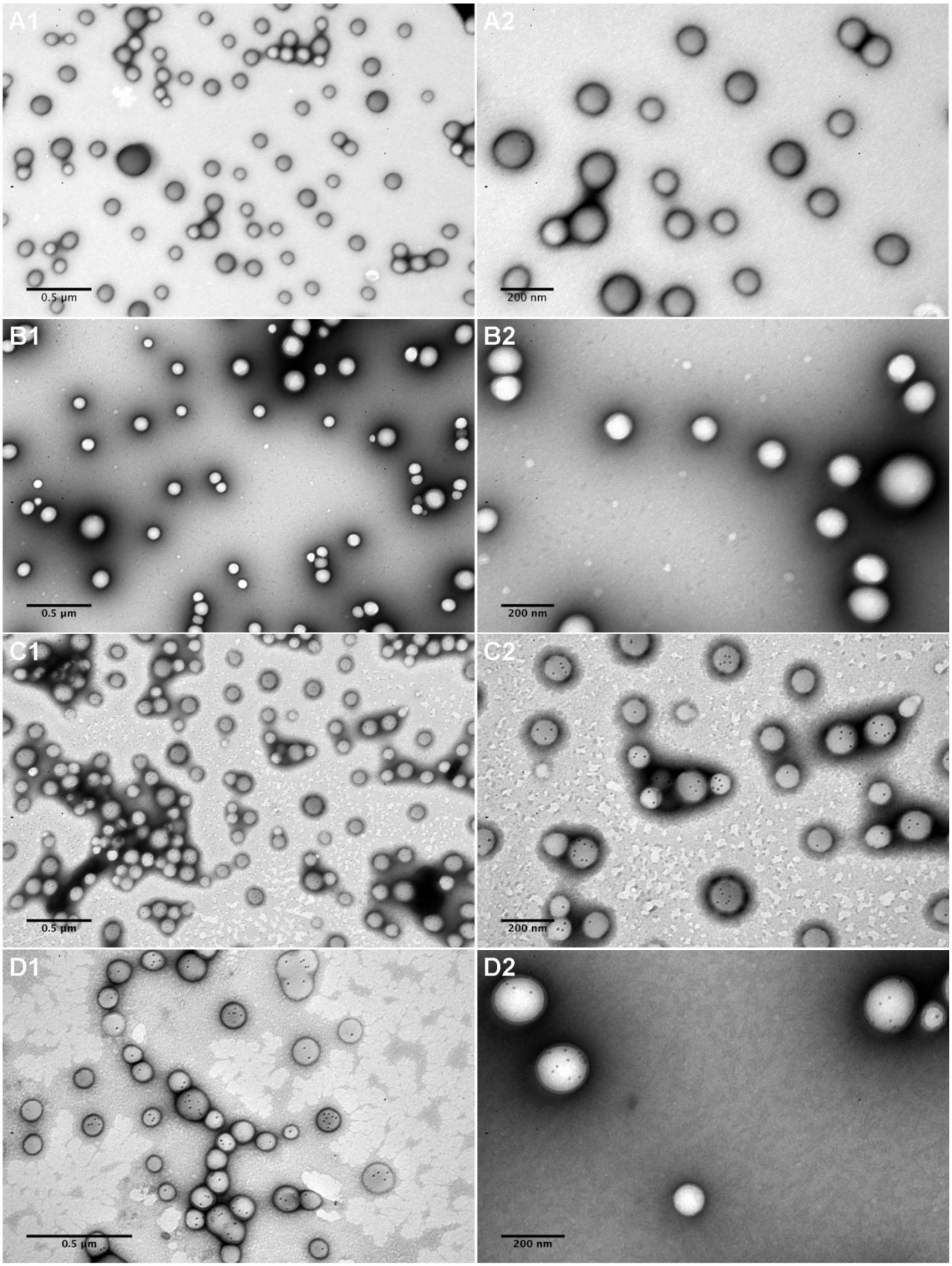

Figure 16 – Transmission electron micrographs of **(A1, A2)** PLGA NPs, **(B1, B2)** MTX-loaded PLGA NPs, **(C1, C2)** SPIONs-loaded PLGA NPs, and **(D1, D2)** MTX- and SPIONs-loaded PLGA NPs. **(A1, B1, C1)** Scale bars correspond to 0.5 µm. Magnification 50,000 x. **(D1)** Scale bar correspond to 0.5 µm. Magnification 80,000 x. **(A2, B2, C2)** Scale bars correspond to 200 nm. Magnification 100,000 x. **(D2)** Scale bar correspond to 200 nm. Magnification 120,000 x.

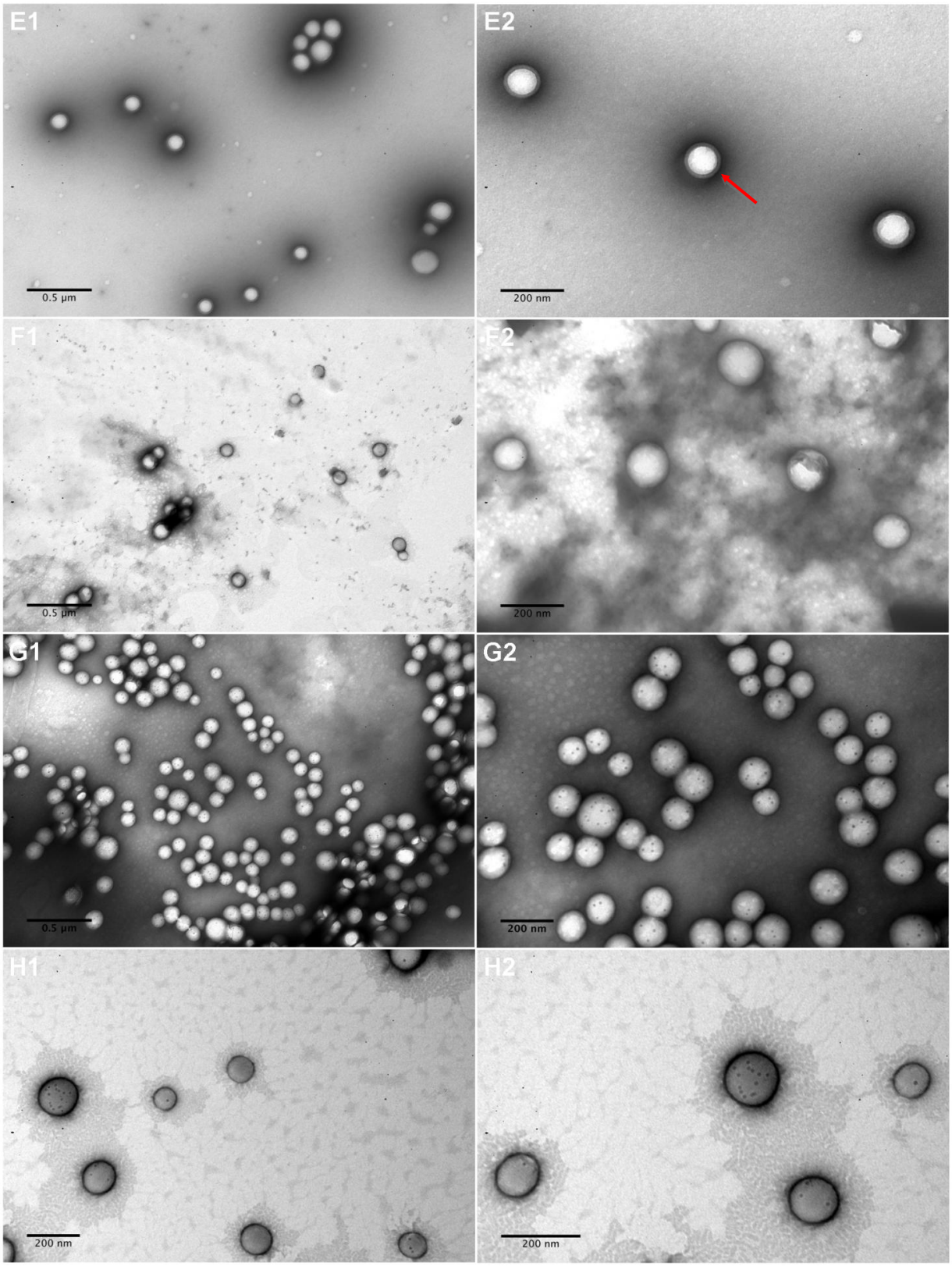

Figure 17 – Transmission electron micrographs of **(E1, E2)** anti-CD64-functionalised PLGA NPs, **(F1, F2**) anti-CD64-functionalised MTX-loaded PLGA NPs, **(G1, G2)** anti-CD64-functionalised SPIONs-loaded PLGA NPs, and **(H1, H2)** anti-CD64-functionalised MTX- and SPIONs-loaded PLGA NPs. In **(E2)** it is possible to detect a 'corona'-like structure typical of surface antibody conjugation (red arrow head). **(E1, F1, G1)** Scale bars correspond to 0.5 µm. Magnification 50,000 x. **(H1)** Scale bar correspond to 200 nm. Magnification 50,000 x. **(E2, F2)** Scale bars correspond to 200 nm. Magnification 120,000 x. **(G2)** Scale bar correspond to 200 nm. Magnification 100,000 x. **(H2)** Scale bar correspond to 200 nm. Magnification 150,000 x.

5.1.4. MTX association efficiency

The FT-IR spectra of PLGA NPs and MTX-loaded PLGA NPs were compared to the FT-IR spectrum of MTX alone (Figure 18). At the wavelength of 1750 cm^{-1}, a marked peak elicits the presence of a carbonyl bond (C=O stretching vibration), which is characteristic of PLGA [80]. Furthermore, on the MTX spectrum, it is possible to observe a different peak at 1638 cm^{-1} (C=C stretching vibration), which is characteristic of the drug molecule, but not of PLGA [81]. On the MTX-loaded NPs spectrum, the characteristic peak from PLGA was not altered, and the carbon-carbon double bond typical of MTX is now also evident on the spectrum, confirming that the MTX was successfully encapsulated into the PLGA NPs.

To quantify MTX encapsulation, the HPLC method previously described allowed demonstrating a high efficiency of association. For MTX-loaded PLGA NPs, the association efficiency was approximately 98%, while for MTX- and SPIONs-loaded PLGA NPs it was around 95% (Table 1). These values did not vary significantly between the two different formulations, indicating that a successful application of co-encapsulation of both agents may be possible in a PLGA-based theranostics approach.

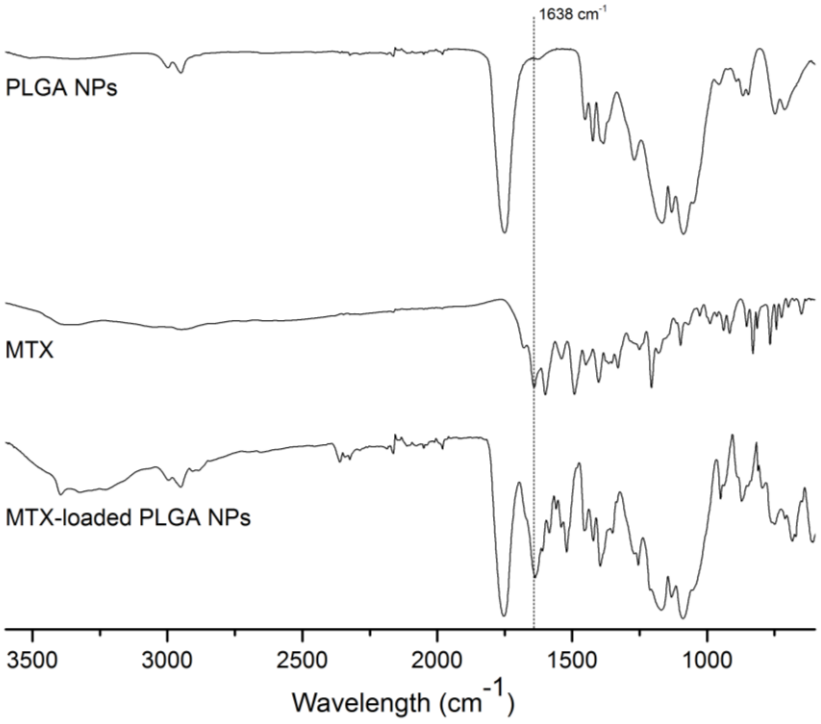

Figure 18 – FT-IR spectra of PLGA NPs, free MTX, and MTX-loaded PLGA NPs.

5.1.5. Antibody conjugation

The FT-IR spectra of PLGA NPs and the anti-CD64-conjugated PLGA NPs were compared to the FT-IR spectrum of the antibody (Figure 19). Once again, at the wavelength of 1750 cm^{-1}, a marked peak elicits the presence of the PLGA-characteristic carbonyl group, which is also present in the Ab (C=O stretching bond [80]). Theoretically, near 1640 cm^{-1} an amide bond (C=N stretching vibration) can be identified regarding the identification of the antibody conjugation to PLGA NPs. However, at 1640 cm^{-1}, both PLGA NPs and anti-CD64 spectra also show a clear peak, which corresponds to another C=O stretching bond on both components [81, 82], not allowing to immediately draw conclusions on the conjugation of the NPs. Despite this, in the anti-CD64 spectrum an additional peak at 1560 cm^{-1} appears, corresponding to the amine groups of the antibody (N-H bending vibrations [82]). In the case of the anti-CD64 conjugated NPs spectrum, this characteristic peak stands out, reflecting the establishment of the antibody conjugation on the surface of the NP.

The antibody conjugation efficiency was also assessed by quantifying the protein amount on the surface of the conjugated NPs. Values of conjugation ranged from approximately 14 to 30 % (Table 1), which is in agreement to values obtained in similar studies [50, 51, 83]. The statistical analysis of the conjugation efficiencies did not show significant differences among formulations, supporting that both MTX and SPIONs encapsulation do not considerably affect the NPs main features and interaction with the antibody. The high standard deviation values can be justified by the fact that the Thermo-Scientific Micro BCA Assay Kit, used for antibody quantification and described in the section 4.2.2.6, despite having a linear working range from 0.5 to 20 µg/mL, only accurately detects protein amounts down to 2 µg/mL when performing the microplate procedure [71]. Therefore, the assay may lose sensitivity when analysing protein amounts near the limits of its detection range. Thorough studies changing the antibody:NPs ratio, as well as the particle activation protocol steps, with EDC and NHS, could help to optimise the antibody-conjugation process aiming at even higher values of efficiency to achieve further functionalised NPs and demanding the use of lower amounts of the antibody.

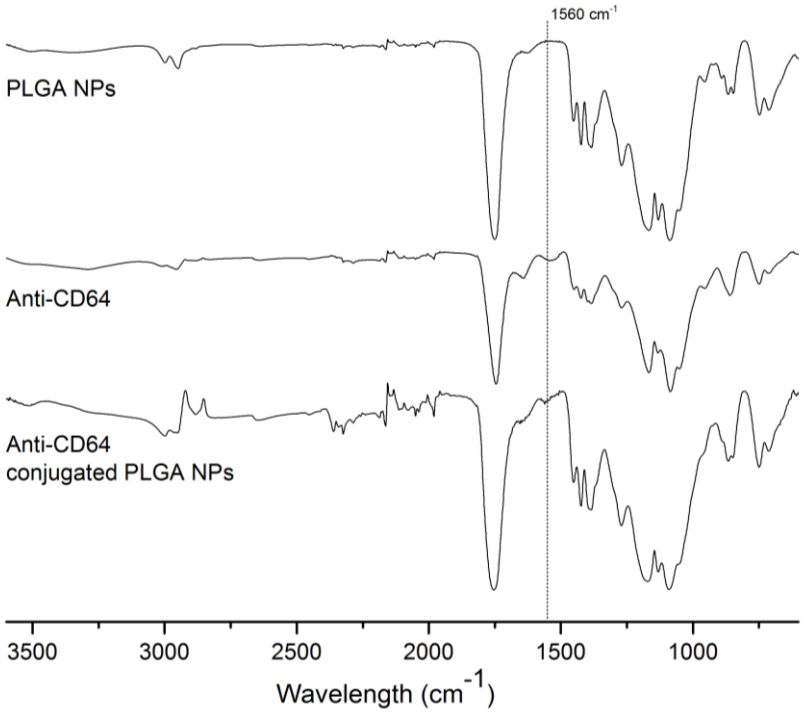

Figure 19 – FT-IR spectra of PLGA NPs, free anti-CD64 antibody, and anti-CD64-conjugated PLGA NPs.

5.2. *In Vitro* Studies

5.2.1. Effect of NPs on cell viability and cytotoxicity

To evaluate the cytotoxicity of the developed NPs, MTT and LDH assays were performed on the macrophage cell line RAW 264.7. On both tests, the assayed values of cells incubated with the nanoparticle formulations were compared to the untreated control, in which only culture medium was added to the wells. Regarding the cytotoxicity of the developed NPs, on the one hand, it is presumable that PLGA and SPIONs-loaded PLGA NPs present no cell toxicity, since they are described as being biocompatible nanocarriers [29, 36, 84]. On the other hand, it is expected that MTX-loaded nanosystems present cytotoxicity, since MTX disrupts cellular folate metabolism hence decreasing cell proliferation [85].

Focusing on the MTT assay (Figure 20), one can observe that only the highest concentration tested (1 mg/mL) presented, up to some extent, cytotoxicity to RAW 264.7 cells, in all NP formulations. Considering all other lower concentrations tested, only the NPs which encapsulated the cell-toxic MTX drug caused a significant reduction (presenting p-values frequently lower than 0.01) on the levels of cell metabolism and proliferation, coming into agreement to what has been anticipated. These results are further corroborated by the LDH assay, in which the toxicity of MTX stands out immediately and is evidenced in Figure 21. Once again, one could observe that only at the highest concentration did all formulations present some toxicity to RAW 264.7 cells. Antibody conjugation did not represent higher cytotoxicity of all NP formulations when compared to non-conjugated NPs. This is justified by the fact that RAW 264.7 macrophages do not express the human CD64 receptor, for which the used antibody is specific. In future work, using a human macrophage cell line, THP-1, one can hope to witness a higher toxicity of the functionalised NPs, suggesting a specific and targeted effect on macrophages over-expressing the CD64 receptor, found in RA. Further studies regarding the incubation of SPIONs, the anti-CD64 antibody, and MTX alone with RAW 264.7 cells would allow to totally confirm the biocompatibility of the two former, as well as the cytotoxicity of the latter.

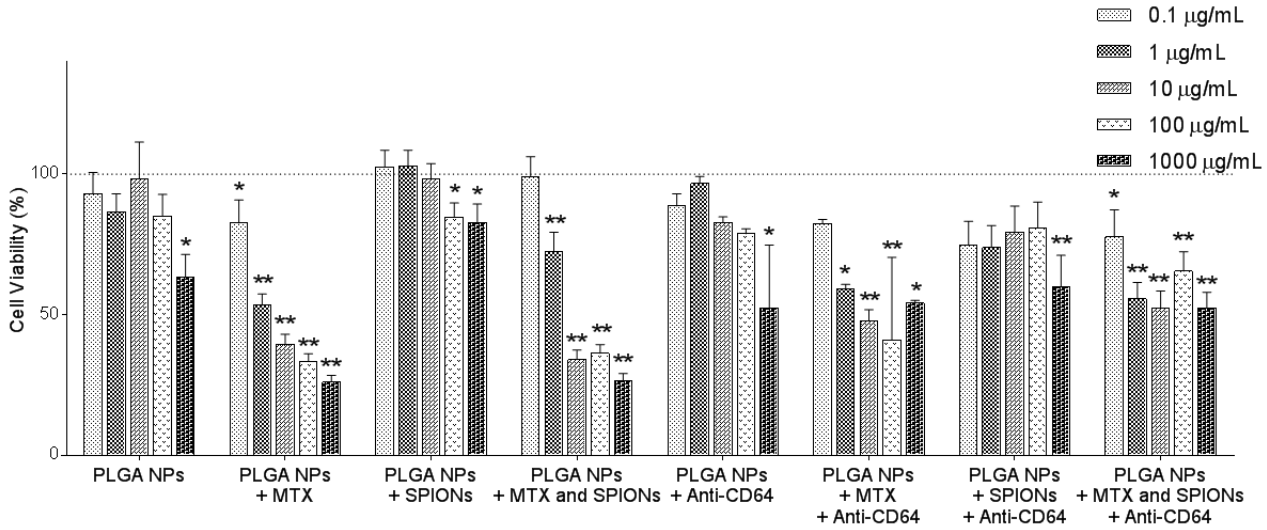

Figure 20 – Effect of the devised NPs on RAW 264.7 macrophage cells viability as a function of the different formulations and concentrations (0.1, 1, 10, 100 and 1000 μg/mL) tested. Cells were incubated with the NPs for 24h and the cell viability assessed by the MTT assay. Values represent mean ± SD (n≥3; *p <0.05; **p <0.01).

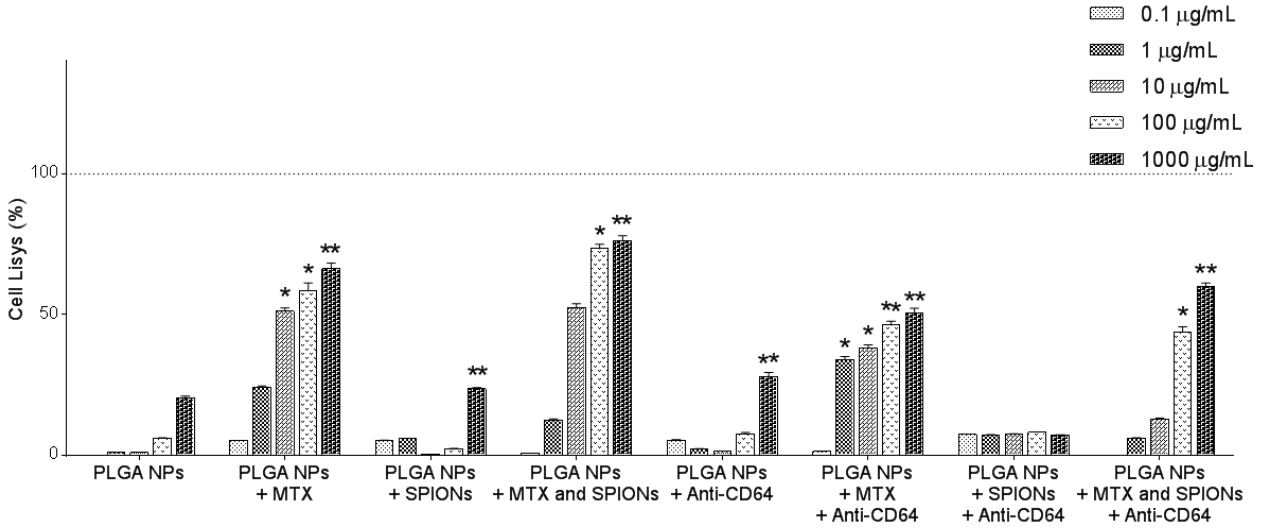

Figure 21 – Cytotoxicity of the devised NPs on RAW 264.7 macrophage cells as a function of the different formulations and concentrations (0.1, 1, 10, 100 and 1000 μg/mL) tested. Cells were incubated with the NPs for 24h and their cytotoxicity assessed by the LDH assay. Values represent mean ± SD (n≥3; *p <0.05; **p <0.01).

5.2.2. Uptake studies

Regarding the uptake of the NP formulations into RAW 264.7 cells, preliminary HPLC quantification demonstrate that macrophages have taken up higher MTX amounts when formulated into NPs. These results support what has been observed at the inverted optical microscope after the 4 and 6 hours incubation time-points with free MTX and MTX-loaded NPs, in which a higher cell death could be observed when RAW 264.7 were treated with the NPs, proving the efficacy of the system. The HPLC results are currently being confirmed by the realisation of more replicate studies.

For this work, cytotoxicity and cell viability studies were envisioned for two different cells lines, RAW 264.7 – a murine macrophage cell line – and THP-1 – a human acute monocytic leukemia-derived monocyte cell line, which can be later differentiated into macrophages, by induction through the addition of phorbol 12-myristate 13-acetate (PMA). While both would allow assessing the cytotoxicity of the developed PLGA NPs, and that this toxicity was given to the drug in study (MTX), the human cell line (THP-1) would allow for the confirmation of a higher cellular uptake and consequent cytotoxicity of anti-CD64-conjugated NPs on THP-1, once this antibody is specific to the human Fc receptor CD64 [86], but not for murine. The comparison of the cellular uptake between cell lines would prove the specificity of the targeted therapy for the diseased RA-cells (over-expressing CD64), which would allow minimizing damage to the surrounding healthy tissues, in an *in vivo* approach. Studies with the THP-1 cell line are currently on-going aiming for a future publication.

Conclusions

Multifunctional PLGA-based nanocarriers for drug targeting and *in vivo* imaging are of particular interest due to their biodegradability and biocompatibility. In this work, a bold attempt to achieve targeted therapy and imaging of RA was devised, by co-encapsulation of both MTX and SPIONs into PLGA NPs, which were further functionalised with anti-CD64, the specific antibody for the overly-expressed macrophage cell surface receptor in RA.

The studied NPs aiming for a new RA-therapy and imaging strategy produced remarkable results in terms of both their physicochemical features as well as their behaviour in the conducted *in vitro* studies with the murine macrophage cell line – RAW 264.7. Regarding particle size, NPs presented sizes comprised within the range of 135-200 nm and with homogeneous distributions, demonstrating great potential for intravenous administration. Through scanning and transmission electron microscopy it was possible to confirm these results and also to assess the NPs morphology. The NPs presented spherical and uniform shape, with a smooth surface.

Zeta potential values ranged from approximately -16 to -32 mV, justified by the presence of the negatively-charged carboxyl termini at the surface of PLGA NPs, which help stabilizing NPs in suspension. Particle size and zeta potential were not significantly affected by neither MTX nor SPIONs encapsulation. However, antibody conjugation caused an expected slight increase in particle size and a decrease in the surface charge, maintaining, nevertheless, the PLGA NPs characteristic features.

The first proof of successful MTX and SPIONs encapsulation was visible with the naked eye, with the formulations presenting different colours and aspect even after extensive rinsing of the exceeding reagents. MTX encapsulation was further confirmed by FT-IR spectroscopy studies which identified the characteristic transmittance peak of the drug in MTX-loaded PLGA NPs. Later, MTX was quantified by HPLC rendering an association efficiency as high as 95%. SPIONs encapsulation, in its turn, was clearly visible through TEM analysis which exhibited micrographs showing small, denser spots incorporated in the polymeric particle.

Regarding the targeting ability of PLGA NPs, the anti-CD64 antibody conjugation was confirmed by FT-IR spectroscopy studies, which identified the characteristic peak of the amine bond of the antibody in functionalised NPs. The conjugation efficiency was assessed by quantifying the antibody present on PLGA-based nanosystems, reaching values between 15 and 30%.

Additionally, *in vitro* studies on the effect of the developed PLGA NPs on RAW 264.7 cells were conducted. PLGA-NPs without MTX were not toxic to the RAW 264.7 cells, with exception to the higher tested concentration. Contrarily, MTX-loaded NPs affected cell's viability after 24 hours of NPs incubation, confirming the MTX cytotoxicity.

To conclude, the attained results suggest that the devised formulations show a huge potential for targeting RA *in vivo*, aiming to both deliver a therapeutic agent while providing enhanced imaging contrast for techniques such as MRI. However, there is always room for improvement, and further and more comprehensive studies should be conducted for nanotechnology approaches of this kind to become a reality in the clinical practice of RA therapy.

- This Page was intentionally left blank. -

Future work

For future work, regarding NP characterisation, magnetisation studies can be conducted to prove the magnetic profile of SPION-encapsulated PLGA NPs. This behaviour can be observed, for instance, via hysteresis loop or magnetisation curve analyses [63, 87], and is important when thinking on the NPs when used as a MRI contrast agent. *In* vitro MRI studies can also be conducted to assess the devised NPs potential to work as a diagnosis agent [88], and allowing the optimisation of the most appropriate SPIONs concentration to be used.

Still on the subject of the NPs characterisation, lyophilisation can be crucial for sample preparation for a correct SEM analysis. Moreover, freeze-dried NPs could provide a good solution for stable NP storage, on the long term. Therefore, a freeze-dried protocol that does not compromise the NPs structure and physico-chemical properties needs optimising.

On a different perspective, it would be relevant to optimise the NPs functionalisation with the anti-CD64 antibody. By changing the anti-CD64:NPs ratio, the conjugation process could be improved, pointing for the use of lower amounts of antibody, avoiding waste. Additionally, a more comprehensive study should be directed to the targeting efficacy and internalisation of the devised NPs. Taking into consideration cellular uptake, NPs can be further functionalised with a hydrophilic polymer providing stealthness, aiming to both increase their blood circulation time and to promote cellular internalisation [29, 31].

Studying the cytotoxicity of free MTX on macrophage cells can allow drawing complementary conclusions on the cytotoxicity of PLGA NPs, and how MTX cytotoxicity augments with the use of the devised NPs as a vehicle. This internalisation of MTX through the use of NPs could also be assessed resourcing to additional techniques such as fluorescence microscopy or flow cytometry. Furthermore, *in vitro* studies should be performed in different cell lines to prove the specificity of the targeted therapy for cells expressing the CD64 cell surface receptor. Ultimately, the efficacy of the optimized nanoparticulate systems must be tested *in vivo* in a disease animal model.

- This Page was intentionally left blank. -

References

1. Kumar, P and Clark, ML, *Kumar & Clark's Clinical Medicine*. 7th ed. 2009.

2. Ross, M and Pawlina, W, *Histology, A Text and Atlas*. 6th ed. 2011.

3. Firestein, GS, *Etiology and pathogenesis of rheumatoid arthritis*, in *Kelley's Textbook of Rheumatology*. 2005.

4. Schmidt, TA, Gastelum, NS, Nguyen, QT, Schumacher, BL, Sah, RL, *Boundary lubrication of articular cartilage: Role of synovial fluid constituents.* Arthritis & Rheumatism, 2007. **56**(3): p. 882-891.

5. Davis, JM and Matteson, EL, *My Treatment Approach to Rheumatoid Arthritis.* Mayo Clinic Proceedings, 2012. **87**(7): p. 659-673.

6. Firth, J, *Treating to target in rheumatoid arthritis.* Nurse Prescribing, 2007. **10**(6): p. 293-302.

7. Firth, J., *Rheumatoid arthritis: diagnosis and multidisciplinary management.* British Journal of Nursing, 2011. **20**(18): p. 1179-80, 1182, 1184-5.

8. Firestein, GS, *Starving the synovium: angiogenesis and inflammation in rheumatoid arthritis.* Journal of Clinical Investigation, 1999. **103**(1): p. 3-4.

9. Liu, H and Pope, RM, *The role of apoptosis in rheumatoid arthritis.* Current Opinion in Pharmacology, 2003. **3**(3): p. 317-22.

10. Choy, EH and Panayi, GS, *Cytokine pathways and joint inflammation in rheumatoid arthritis.* The New England Journal of Medicine, 2001. **344**(12): p. 907-16.

11. Pope, RM, *Apoptosis as a therapeutic tool in rheumatoid arthritis.* Nature Reviews Immunology, 2002. **2**(7): p. 527-35.

12. Koch, AE, *Angiogenesis as a target in rheumatoid arthritis.* Annals of the Rheumatic Diseases, 2003. **62 (2)**: p. ii60-7.

13. Smolen, JS and Steiner, G, *Therapeutic strategies for rheumatoid arthritis.* Nature Reviews Drug Discovery, 2003. **2**(6): p. 473-88.

14. Majithia, V. and S.A. Geraci, *Rheumatoid arthritis: diagnosis and management.* The American Journal of Medicine, 2007. **120**(11): p. 936-9.

15. McQueen, FM, *Magnetic resonance imaging in early inflammatory arthritis: what is its role?* Rheumatology, 2000. **39**(7): p. 700-6.

16. Brown, A, Wakefield, R, Conaghan, P, Karim, Z, O'Connor, P and Emery, P, *New approaches to imaging early inflammatory arthritis.* Clinical and Experimental Rheumatology, 2004. **22**(5 Suppl 35): p. S18-25.

17. Chen, Y, Tsai, C, Huang, P, Chang, M, Cheng, P, Chou, C, Chen, D, Wang, C, Shiau, A and Wu, C, *Methotrexate conjugated to gold nanoparticles inhibits tumor growth in a syngeneic lung tumor model.* Molecular Pharmacology, 2007. **4**(5): p. 713-22.

18. Tian, H and Cronstein BN, *Understanding the mechanisms of action of methotrexate: implications for the treatment of rheumatoid arthritis.* Bulletin of the NYU Hospital for Joint Diseases, 2007. **65**(3): p. 168-73.

19. Yazici, Y, Sokka, T, Kautiainen, H, Swearingen, C, Kulman, I and Pincus, T, *Long term safety of methotrexate in routine clinical care: discontinuation is unusual and rarely the result of laboratory abnormalities.* Annals of the Rheumatic Diseases, 2005. **64**(2): p. 207-11.

20. Ferrari, M, *Cancer nanotechnology: opportunities and challenges.* Nature Reviews Cancer, 2005. **5**(3): p. 161-71.

21. Blanco, E, Hsiao, A, Mann, A, Landry, M, Meric-Bernstam, F, and Ferrari, M, *Nanomedicine in cancer therapy: innovative trends and prospects.* Cancer Science, 2011. **102**(7): p. 1247-52.

22. Andresen, T, Thompson, D and T. Kaasgaard, *Enzyme-triggered nanomedicine: drug release strategies in cancer therapy.* Molecular Membrane Biology, 2010. **27**(7): p. 353-63.

23. Panyam, J and Labhasetwar, V, *Biodegradable nanoparticles for drug and gene delivery to cells and tissue.* Advanced Drug Delivery Reviews, 2003. **55**(3): p. 329-47.

24. Muthu, MS, Kulkarni, SA, Raju, A and Feng, SS, *Theranostic liposomes of TPGS coating for targeted co-delivery of docetaxel and quantum dots.* Biomaterials, 2012. **33**(12): p. 3494-3501.

25. Yuan, Q, Hein, S and Misra, RD, *New generation of chitosan-encapsulated ZnO quantum dots loaded with drug: synthesis, characterization and in vitro drug delivery response.* Acta Biomaterialia, 2010. **6**(7): p. 2732-9.

26. Muthu, MS and Feng, SS, *Theranostic liposomes for cancer diagnosis and treatment: current development and pre-clinical success.* Expert Opinion Drug Delivery, 2013. **10**(2): p. 151-5.

27. Ling, Y, Wei, K, Luo, Y,Gao, X and Zhong, S, *Dual docetaxel/superparamagnetic iron oxide loaded nanoparticles for both targeting magnetic resonance imaging and cancer therapy.* Biomaterials, 2011. **32**(29): p. 7139-50.

28. Yu, MK, Jeong, Y Y, Park, J, Park, S, Kim, JW, Min, JJ, Kim, K and Jon, S, *Drug-loaded superparamagnetic iron oxide nanoparticles for combined cancer imaging and therapy in vivo.* Angewandte Chemie (International ed. in English), 2008. **47**(29): p. 5362-5.

29. Danhier, F, Ansorena, E, Silva, JM, Coco, R, Le Breton, A and Preat, V, *PLGA-based nanoparticles: an overview of biomedical applications.* Journal of Controlled Release, 2012. **161**(2): p. 505-22.

30. Ratner, BD, Allan, SH, Frederick JS and Jack EL, *Biomaterials Science - An Introduction to Materials in Medicine*. 2nd ed. 2004.

31. Kumari, A., Yadav, SK and Yadav, SC, *Biodegradable polymeric nanoparticles based drug delivery systems.* Colloids and Surfaces B: Biointerfaces, 2010. **75**(1): p. 1-18.

32. Bala, I, Hariharan, S and Kumar, M, *PLGA nanoparticles in drug delivery: the state of the art.* Critical Reviews in Therapeutic Drug Carrier Systems, 2004. **21**(5): p. 387-422.

33. Biomaterials, P. *Product Information Sheet for PLGA*. 2012; Available from: http://www.puracbiomaterials.com].

34. Stephen, ZR, Kievit, FM and Zhang, M, *Magnetite Nanoparticles for Medical MR Imaging.* Materials Today, 2011. **14**(7-8): p. 330-338.

35. Chao, Y, Makale, M, Karmali, P, Sharikov, Y, Tsigelny, I, Merkulov, S, Kesari, S, Wrasidlo, W, Ruoslahti, E and Simberg, D, *Recognition of Dextran–Superparamagnetic Iron Oxide Nanoparticle Conjugates*

(Feridex) via Macrophage Scavenger Receptor Charged Domains. Bioconjugate Chemistry, 2012. **23**(5): p. 1003-1009.

36. Figuerola, A, Di Corato, R, Manna, L and Pellegrino, T, *From iron oxide nanoparticles towards advanced iron-based inorganic materials designed for biomedical applications.* Pharmaceutical Research, 2010. **62**(2): p. 126-43.

37. Rosen, JE, Chan, L, Shieh, D B and Gu, F X, *Iron oxide nanoparticles for targeted cancer imaging and diagnostics.* Nanomedicine, 2012. **8**(3): p. 275-90.

38. Mahmoudi, M, Sun, Y, Zheng, Y, Ran, H, Zhou, Y, Shen, H, Chen, Y, Chen, H, Krupka, Tianyi, M, Li, A, Li, P, Wang, Z and Wang, Z, *Superparamagnetic iron oxide nanoparticles (SPIONs): development, surface modification and applications in chemotherapy.* Advanced Drug Delivery Reviews, 2011. **63**(1-2): p. 24-46.

39. Gupta, AK and Gupta, M *Synthesis and surface engineering of iron oxide nanoparticles for biomedical applications.* Biomaterials, 2005. **26**(18): p. 3995-4021.

40. Hekimoglu, K, Hekimoglu, K, Ustundag, Y, Dusak, A, Kalaycioglu, B, Besir, H, Engin, H and Erdem, O, *Small colorectal liver metastases: Detection with SPIO-enhanced MRI in comparison with gadobenate dimeglumine-enhanced MRI and CT imaging.* European Journal of Radiology, 2011. **77**(3): p. 468-472.

41. AMAG Pharmaceuticals, I. *Feridex I.V.*®. Available from: http://www.amagpharma.com/documents/products/pdfs/feridex_insert.pdf].

42. Butoescu, N, Seemayer, CA, Foti, M, Jordan, O, and Doelker, E, *Dexamethasone-containing PLGA superparamagnetic microparticles as carriers for the local treatment of arthritis.* Biomaterials, 2009. **30**(9): p. 1772-80.

43. Cardoso, M, Peca, I and Roque, A, *Antibody-conjugated nanoparticles for therapeutic applications.* Current Medicinal Chemistry, 2012. **19**(19): p. 3103-27.

44. Fay, F and Scott, CJ, *Antibody-targeted nanoparticles for cancer therapy.* Immunotherapy, 2011. **3**(3): p. 381-94.

45. Beck, A, Wurch, T, Bailly, C and Corvaia, N., *Strategies and challenges for the next generation of therapeutic antibodies.* Nature Reviews Immunology, 2010. **10**(5): p. 345-52.

46. Liu, Y, Miyoshi, H, and Nakamura, M, *Nanomedicine for drug delivery and imaging: a promising avenue for cancer therapy and diagnosis using targeted functional nanoparticles.* International Journal of Cancer, 2007. **120**(12): p. 2527-37.

47. Burstein, S and Knapp, R, *Chemotherapy of murine ovarian carcinoma by methotrexate-antibody conjugates.* Journal of Medicinal Chemistry, 1977. **20**(7): p. 950-2.

48. Arruebo, M, Valladares, M and Gonzalez-Fernandez, A, *Antibody-conjugated nanoparticles for biomedical applications.* Journal of Nanomaterials, 2009. **2009**: p. 1-24.

49. Xu, H, Aguilar, ZP, Yang, L, Kuang, M, Duan, H, Xiong, Y, Wei, H and Wang, A, *Antibody conjugated magnetic iron oxide nanoparticles for cancer cell separation in fresh whole blood.* Biomaterials, 2011. **32**(36): p. 9758-65.

50. Scott, CJ, Marouf, WM, Quinn, DJ, Buick, RJ, Orr, SJ, Donnelly, RF and McCarron, P A, *Immunocolloidal targeting of the endocytotic siglec-7 receptor using peripheral attachment of siglec-7 antibodies to poly(lactide-co-glycolide) nanoparticles.* Pharmaceutical Research, 2008. **25**(1): p. 135-46.

51. Kocbek, P, Obermajer, N, Cegnar, M, Kos, J and Kristl, J., *Targeting cancer cells using PLGA nanoparticles surface modified with monoclonal antibody.* Journal of Controlled Release, 2007. **120**(1-2): p. 18-26.

52. McCarron, PA, Marouf, WM, Quinn, DJ, Fay, F, Burden, RE, Olwill, SA and Scott, CJ, *Antibody targeting of camptothecin-loaded PLGA nanoparticles to tumor cells.* Bioconjug Chem, 2008. **19**(8): p. 1561-9.

53. Jain, NK, Mishra, V and Mehra, NK, *Targeted drug delivery to macrophages.* Expert Opinion on Drug Delivery, 2013.

54. Taylor, PR, Martinez-Pomares, L, Stacey, M, Lin, H-H, Brown, GD and Gordon, S *Macrophage Receptors and Immune Recognition.* Annual Review of Immunology, 2005. **23**: p. 901-944.

55. Nahar, M, Dubey, V, Mishra, D, Mishra, PK, Dube, A, Jain, NK, *In vitro evaluation of surface functionalized gelatin nanoparticles for macrophage targeting in the therapy of visceral leishmaniasis.* Journal of Drug Targeting, 2010. **18**(2): p. 93-105.

56. Nahar, M and Jain, NK, *Preparation, characterization and evaluation of targeting potential of amphotericin B-loaded engineered PLGA nanoparticles.* Pharmaceutical Research, 2009. **26**(12): p. 2588-98.

57. Nimje, N, Agarwal, A, Saraogi, GK, Lariya, N, Rai, G, Agrawal, H, Agrawal, GP, *Mannosylated nanoparticulate carriers of rifabutin for alveolar targeting.* Journal of Drug Targeting, 2009. **17**(10): p. 777-87.

58. Fueldner, C., Mittag, A, Knauer, J, Biskop, M, Hepp, P, Scholz, R, Wagner, U, Sack, U, Emmrich, F, Tarnok, A and Lehmann, J, *Identification and evaluation of novel synovial tissue biomarkers in rheumatoid arthritis by laser scanning cytometry.* Arthritis Research & Therapy, 2012. **14**(1): p. R8.

59. van Vuuren, AJ, van Roon, JA, Walraven, V, Harmsen, MC, McLaughlin, PM and van de Winkel, JG, *CD64-directed immunotoxin inhibits arthritis in a novel CD64 transgenic rat model.* The Journal of Immunology, 2006. **176**(10): p. 5833-8.

60. van Roon, JA, van Vuuren, AJ, Wijngaarden, S, Jacobs, KMG, Bijlsma, JWJ, Lafeber, FPJG, Thepen, T, and van de Winkel, JG *Selective Elimination of Synovial Inflammatory Macrophages in Rheumatoid Arthritis by an Fc-gamma Receptor I–Directed Immunotoxin.* Arthritis & Rheumatism, 2003. **48**(5): p. 1229–1238.

61. Keler, T, Guyre, PM, Vitale LA, Sundarapandivan, K, van de Winkel, JG and Graziano, RF, *Targeting weak antigens to CD64 elicits potent humoral responses in human CD64 transgenic mice.* The Journal of Immunology 2000. **165**(12): p. 6738-42.

62. Sarmento, B, Martins, S, Ferreira, D and Souto, E, *Oral insulin delivery by means of solid lipid nanoparticles*. International Journal of Nanomedicine, 2007. 2(4): p. 743-749.

63. Butoescu, N, Jordan, O, Burdet, P, Stadelmann, P, Petri-Fink, A, Hofmann, H and Doelker, E, *Dexamethasone-containing biodegradable superparamagnetic microparticles for intra-articular administration: physicochemical and magnetic properties, in vitro and in vivo drug release.* European Journal of Pharmaceutics and Biopharmaceutics, 2009. **72**(3): p. 529-38.

64. Silva, MF, Winkler Hechenleitner, AA, de Oliveira, DM, Agueros, M, Penalva, R, Irache, JM and Pineda, EA, *Optimization of maghemite-loaded PLGA nanospheres for biomedical applications.* European Journal of Pharmaceutical Sciences, 2013. **49**(3): p. 343-51.

65. Information, N.C.f.B. *PubChem Compound: Methotrexate*. Available from: http://pubchem.ncbi.nlm.nih.gov/summary/summary.cgi?cid=126941&loc=ec_rcs].

66. Swanson, JA. and Hoppe, AD, *The coordination of signaling during Fc receptor-mediated phagocytosis.* Journal of Leukocyte Biology, 2004. **76**(6): p. 1093-103.

67. Malvern Instruments, L., *DLS Technical Note - Dynamic Light Scattering: An introduction in 30 minutes.*

68. Malvern Instruments, L., *Zeta Potential: An introduction in 30 Minutes:* .

69. Sartori, T, Murakami, FS, Cruz, AP, and Campos, AM, *Development and validation of a fast RP-HPLC method for determination of methotrexate entrapment efficiency in polymeric nanocapsules.* Journal of Chromatographic Science, 2008. **46**(6): p. 505-9.

70. Trapani, A, Denora, N, Iacobellis, G, Sitterberg, J, Bakowsky, U and Kissel, T, *Methotrexate-loaded chitosan- and glycol chitosan-based nanoparticles: a promising strategy for the administration of the anticancer drug to brain tumors.* AAPS PharmSciTech, 2011. **12**(4): p. 1302-11.

71. Inc., T.F.S. *Instructions: Micro BCA™ Protein Assay Kit.* 2013; http://www.piercenet.com/instructions/2160412.pdf].

72. ATCC®. *RAW 264.7 (ATCC® TIB-71™)*. http://www.lgcstandards-atcc.org/Products/All/TIB-71.aspx].

73. Mosmann, T, *Rapid colorimetric assay for cellular growth and survival: Application to proliferation and cytotoxicity assays.* Journal of Immunological Methods, 1983. **65**(1–2): p. 55-63.

74. Inc., T.B. *MK401, LDH Cytotoxicity Detection Kit*. http://www.takara-bio.com].

75. das Neves, J, Michiels, J, Arien, KK, Vanham, F, Amiji, M, Bahia, MF and Sarmento, B., *Polymeric nanoparticles affect the intracellular delivery, antiretroviral activity and cytotoxicity of the microbicide drug candidate dapivirine.* Pharmaceutical Research, 2012. **29**(6): p. 1468-84.

76. Moghimi, SM, Hunter, AC and Murray, JC, *Long-circulating and target-specific nanoparticles: theory to practice.* Pharmacological Reviews, 2001. **53**(2): p. 283-318.

77. Cho, K, Wang, X, Nie, S, Chen, Z and Shin, D, *Therapeutic nanoparticles for drug delivery in cancer.* Clinical Cancer Research, 2008. **14**(5): p. 1310-6.

78. Kedmi, R., Ben-Arie, N and Peer, D, *The systemic toxicity of positively charged lipid nanoparticles and the role of Toll-like receptor 4 in immune activation.* Biomaterials, 2010. **31**(26): p. 6867-6875.

79. Thamake, S.I., et al., *Surface functionalization of PLGA nanoparticles by non-covalent insertion of a homo-bifunctional spacer for active targeting in cancer therapy.* Nanotechnology, 2011. **22**(3): p. 035101.

80. Choi, S-W and Kim, J-H, *Design of surface-modified poly(d,l-lactide-co-glycolide) nanoparticles for targeted drug delivery to bone.* Journal of Controlled Release, 2007. **122**(1): p. 24-30.

81. Kohler, N, Sun, C, Wang, J and Zhang, M, *Methotrexate-modified superparamagnetic nanoparticles and their intracellular uptake into human cancer cells.* Langmuir, 2005. **21**(19): p. 8858-64.

82. Sarmento, B, Ferreira, D, Veiga, F and Ribeiro, A, *Characterization of insulin-loaded alginate nanoparticles produced by ionotropic pre-gelation through DSC and FTIR studies.* Carbohydrate Polymers, 2006. **66**(1): p. 1-7.

83. Cirstoiu-Hapca, A, Bossy-Nobs, L, Buchegger, F, Gurny, R and Delie, F, *Differential tumor cell targeting of anti-HER2 (Herceptin®) and anti-CD20 (Mabthera®) coupled nanoparticles.* International Journal of Pharmaceutics, 2007. **331**(2): p. 190-196.

84. Silva, JM, Videira, M, Gaspar, R, Preat, V and Florindo, HF, *Immune system targeting by biodegradable nanoparticles for cancer vaccines.* Journal of Controlled Release, 2013. **168**(2): p. 179-99.

85. Lindgren, M, Rosenthal-Aizman, K, Saar, K, Eiriksdottir, E, Jiang, Y, Sassian, M, Ostlund, P, Hallbrink, M and Langel, U, *Overcoming methotrexate resistance in breast cancer tumour cells by the use of a new cell-penetrating peptide.* Biochemical Pharmacology, 2006. **71**(4): p. 416-25.

86. Fleit, HB and Kobasiuk, CD, *The human monocyte-like cell line THP-1 expresses Fc gamma RI and Fc gamma RII.* Journal of Leukocyte Biology, 1991. **49**(6): p. 556-65.

87. Niu, C, Wang, Z, Lu, G, Krupka, TM, Sun, Y, You, Y, Song, W, Ran, H, Li, P and Zheng, Y, *Doxorubicin loaded superparamagnetic PLGA-iron oxide multifunctional microbubbles for dual-mode US/MR imaging and therapy of metastasis in lymph nodes.* Biomaterials, 2013. **34**(9): p. 2307-17.

*88. Sun, Y, Zheng, Y, Ran, H, Zhou, Y, Shen, H, Chen, Y, Chen, H, Krupka, TM, Li, A, Li, P and Wang, Z, Superparamagnetic PLGA-iron oxide microcapsules for dual-modality US/MR imaging and high intensity focused US breast cancer ablation. Biomaterials, 2012. **33**(24): p. 5854-5864.*